

# **The impacts of inter-El Nino variability on the Tropical Atlantic and Northeast Brazil climate**

Regina R. Rodrigues  
Oceanographic Institute, University of São Paulo, São Paulo

Reindert J. Haarsma  
Royal Netherlands Meteorological Institute, De Bilt

Edmo J. D. Campos  
Oceanographic Institute, University of São Paulo, São Paulo

Tércio Ambrizzi  
Department of Atmospheric Sciences, University of São Paulo, São Paulo

---

*Corresponding author address:* Regina R. Rodrigues, Instituto Oceanográfico, Universidade de São Paulo, Praça do Oceanográfico 191, São Paulo, SP, 05508-120, Brazil.

E-mail: [regina.rodrigues@usp.br](mailto:regina.rodrigues@usp.br)

## Abstract

In this study, observations and numerical simulations are used to investigate how different El Niño events affect the development of SST anomalies in the Atlantic and how this relates to the Brazilian Northeast (NE) precipitation. Our results show that different types of El Niño have different impacts on the SST anomalies of the equatorial and tropical South Atlantic but a similar SST response in the tropical North Atlantic. Strong and long (weak and short) El Niños with the main heating source located in the eastern (central) Pacific generate cold (warm) anomalies in the cold tongue and Benguela upwelling regions during boreal winter and spring. When the SST anomalies in the eastern equatorial and tropical South Atlantic are cold (warm), the meridional SST gradient across the equator is positive (negative) and the ITCZ is prevented (allowed) to move southward during the boreal spring; as a consequence, the precipitation is below (above) the average over the NE. Thus, strong and long (weak and short) El Niños are followed by dry (wet) conditions in the NE. During strong and long El Niños, changes in both the Walker circulation over the Atlantic and the Pacific-South Atlantic (PSA) wave train cause easterly wind anomalies in the western equatorial Atlantic, which in turn activate the Bjerknes mechanism establishing the cold tongue in boreal spring and summer. These easterly anomalies are also responsible for the Benguela upwelling. During short and weak El Niños, westerly wind anomalies are present in the western equatorial Atlantic accompanied by warm anomalies in the eastern equatorial and tropical South Atlantic; a positive phase of the South Atlantic dipole develops during boreal winter. Our simulations highlight the importance of ocean dynamics in establishing the correct slope of the equatorial thermocline and SST anomalies, which in turn determine the correct rainfall response over the NE.

## 1. Introduction

The variability of the semi-arid climate of the NE is strongly affected by El Niño events. Periods of severe drought tend to occur during El Niño years causing extreme poverty and the subsequent migration of the population to urban centers with major social and political implications. Variations of rainfall over the NE are linked to the position of the ITCZ in the Atlantic (Hastenrath and Heller 1977; Moura and Shukla 1981; Nobre and Shukla 1996). The short rainy season over the NE occurs in the boreal spring from March to May (MAM) when the ITCZ is in its southernmost position. The dominant force driving the ITCZ position and the NE rainfall is locally associated with the meridional Tropical Atlantic SST gradient. In years when the meridional SST gradient is positive (negative) in MAM, i.e., cold (warm) anomalies in the tropical South Atlantic and warm (cold) anomalies in the tropical North Atlantic, the ITCZ is impeded (allowed) to migrate southward and the NE rainfall is below (above) average. During El Niño (La Niña) events, i.e., ENSO warm (cold) phase, the meridional SST gradient generally becomes positive (negative) followed by a dry (wet) rainfall season in the NE during MAM. This ENSO teleconnection is done mainly through the Pacific-North America (PNA) stationary wave bridge (Nobre and Shukla 1996; Hastenrath 2006) and the tropospheric temperature warming over the tropical North Atlantic (Chiang and Lintner 2005; Chang et al. 2006; Grimm and Ambrizzi 2009).

In recent years, it has become clear that specifically during El Niño years the response of the Atlantic meridional SST gradient and consequently the precipitation over the NE can be considerably different. Chang et al. (2006) have shown that El Niño events can be followed by cold and warm events in the equatorial and tropical South Atlantic, in spite of presenting similar well-defined tropospheric warming. Giannini et al. (2004) show for instance that the

meridional SST gradient does not evolve consistently with warm ENSO anomalies. In six out of nine El Niño events during the period 1950-1994, the SST gradient was negative and not positive as expected from the ENSO teleconnection mechanism, leading to different precipitation anomalies over the NE. The variability of the NE precipitation in El Niño years can be related to the preexistent SST anomalies in the Atlantic, reinforcing or hindering the El Niño response in the Atlantic due a constructive/destructive interference between atmospheric and oceanic processes in response to El Niño (Chang et al. 2006; Misra 2006; Barreiro et al. 2005; Giannini et al. 2004).

Several studies have shown that differences in the characteristics of the El Niño event can cause different atmospheric circulation and precipitation responses over India (Kumar et al. 2006), Australia (Wang and Hendon 2007; Taschetto et al. 2009), South Africa (Reason and Jagadheesha 2005), and southern South America (Maganã and Ambrizzi 2005; Silva and Ambrizzi 2006). According to these studies, variations in the location of the heating source from one event to the other are responsible for the precipitation variability. For instance, only El Niño events with the warmest SST anomalies in the central equatorial Pacific generate droughts in India (Kumar et al. 2006), because these events are more effective in focusing drought-producing subsidence over this region than events with the warmest SSTs in the eastern equatorial Pacific (the typical canonical El Niños). There is also some evidence that other characteristics of an El Niño event, such as time evolution and amplitude, can produce different responses in the atmospheric circulation with consequences for precipitation.

The aforementioned considerations have motivated us to revisit the issue of NE rainfall variability during El Niño years, using observations and model simulations (Section 2). Our hypothesis is that the different preexistent tropical Atlantic SST anomalies, and

consequently NE precipitation responses, are caused by inter-El Niño variability. We first investigate differences in the Pacific and Atlantic SST conditions and atmospheric circulation for El Niño years in which the precipitation over the NE is above and below the average from data analysis (Section 3). An atmospheric model is forced with the identified SST patterns to further explore the sensitivity of the NE rainfall to both El Niño and Atlantic SST anomalies, as well as their relative importance (Section 4). The atmospheric model is then coupled to a simple passive mixed layer model (slab ocean) and to an OGCM to determine if different El Niño events can generate different tropical Atlantic SST anomalies and consequently different NE precipitation responses (Section 5). Comparisons between the slab ocean and OGCM runs are presented to establish the role of the ocean dynamics. A summary is given in Section 6.

## 2. Methods

### *a. Data Analysis*

The SST data set used in this study is the monthly Extended Reconstructed SST (ERSST) from 1900 to 2002 (Smith and Reynolds 2004). The El Niño years are defined in a similar fashion to Trenberth (1997), except that here we use normalized NINO3 index (SST anomalies averaged over the Tropical Pacific between  $5^{\circ}\text{N}$ - $5^{\circ}\text{S}$  and  $150^{\circ}\text{W}$ - $90^{\circ}\text{W}$ ), which is better correlated to rainfall anomalies over South America (Grimm and Tedeschi 2009). We use the FUNCEME rainfall dataset (<http://www.funceme.br/areas/monitoramento>) as an estimate for the precipitation over the NE since it is available for 1900-2005 and reproduces the amplitude and temporal variability of the GPCP precipitation (Adler et al. 2003), with a correlation coefficient of 0.91 for the short period of 1979-2005 in which the two timeseries overlap (Fig. 1a). Precipitation was estimated over the area  $10^{\circ}\text{S}$ - $0^{\circ}\text{N}$  and  $50^{\circ}\text{W}$ - $30^{\circ}\text{W}$  using

the GPCP dataset and over Ceará State using the FUNCEME dataset (respectively the solid box and dashed line in the top corner of Fig. 1b). Monthly mean atmospheric fields are taken from the ECMWF-ERA40 reanalysis product for the period 1957-2002. Throughout the paper, the statistical significance of the difference between the mean of the anomalies of the different composites at each grid point is given by a standard two-sample t-test at 95% and 99% confidence levels.

### *b. Model and Experiments*

The atmosphere model used in this study is the Simplified Parameterization Primitive Equation Dynamics (SPEEDY) model (Molteni 2003) with a vertical resolution of seven layers and a triangular spectral truncation at total wavenumber 30 (T30). The model has simplified physics based on a spectral primitive equation core and a set of simplified parameterization schemes, which makes it computationally inexpensive. The parameterization processes include large-scale condensation, convection, clouds, short and long wave radiation, turbulent surface fluxes, and vertical diffusion. The climate simulated by SPEEDY is comparable to that by more complex AGCMs (Molteni 2003). In particular, SPEEDY proved to be a reliable tool for simulating the dominant patterns of variability over the tropical and South Atlantic (Haarsma et al. 2005; Hazeleger and Haarsma 2005), which is vital for this study.

To test if SPEEDY is able to reproduce the main features of the ENSO teleconnection for both DRY and WET conditions (Pacific and Atlantic SST anomalies), we designed a set of ensemble runs of 20 members where the SPEEDY model is integrated for 2 years with prescribed SST anomalies and climatological SST. SST anomaly timeseries are extracted

from the composites for DRY and WET conditions for each month of the El Niño years starting from January of the El Niño onset year to December of the El Niño decay year. The following experiments are conducted: 1) CONTROL run with prescribed climatological SST in both the Pacific and Atlantic; 2) DRY run with prescribed SST anomalies in both the Pacific and Atlantic for DRY conditions; 3) WET run, same as the DRY run, except for WET conditions.

SPEEDY is also integrated with prescribed SST anomalies and climatology in the Pacific while predicting the SST anomalies in the Atlantic using a slab ocean from 45°S to 60°N. These experiments are conducted to investigate if the El Niño predetermines the SST anomalies in the Tropical Atlantic. Three sets of ensemble runs are performed: 1) CONTROL run with prescribed climatological SST in the Pacific; 2) DRY run with prescribed SST anomalies in the Pacific for DRY conditions; and 3) WET run with prescribed SST anomalies in the Pacific for WET conditions. Each ensemble consists of 20 model integrations that are initialized with slightly different conditions to represent internal atmospheric variability. All ensemble runs use a slab ocean in the Atlantic basin starting from a climatological state and are integrated for a 2-year period starting from January of the El Niño onset year to December of the El Niño decay year.

To investigate the role of ocean dynamics, we perform the same set of ensemble runs using SPEEDY fully coupled to the Miami Isopycnal Coordinate Ocean Model (MICOM). The ocean model is configured for the Atlantic basin from 45°S to 60°N with 19 isopycnal layers and a horizontal resolution of 1°. (For more details see Hazeleger and Haarsma, 2005.) The ocean initial state is obtained from a 100-yr climatological run. SPEEDY-MICOM reproduces realistically the climatology and variability of the Tropical Atlantic, including the

east-west tilt of the thermocline along the equator and the variability of the cold tongue and meridional SST gradient.

### **3. Inter-El Niño variability**

#### *a. Atlantic and Pacific SST variability*

Records of precipitation over the NE dating back to 1900 show that during moderate to extreme El Niño years (Fig. 1), there are as many episodes of rainfall below the average as those of rainfall above the average in MAM (“DRY” and “WET” NE cases, respectively). We first examine the 25 El Niño years (1900-2005) for SST conditions in the Atlantic and Pacific that distinguish the 14 DRY from the 11 WET cases. Then we examine 7 DRY cases and 7 WET cases for the 1957-2002 period. The SST anomaly composites for DRY and WET cases extracted from the 1900-2005 period are very similar to those from the 1957-2002 period (Fig. 2). Therefore, we decide to use the shorter period composites from now on for two reasons: 1) the SST data is more reliable for 1957-2002; 2) the atmospheric data set used here is only available for 1957-2002, which ensures consistency throughout our analysis.

There are statistically significant differences between DRY and WET SST composites in the Pacific during the El Niño mature phase (December-February, DJF) and the NE rainy season MAM (Figs. 2c and 2f, respectively). The Pacific warming is stronger for the DRY El Niño years, particularly east of 120°W in DJF where the SST difference reaches 0.7°C. In MAM, the eastern Pacific warming is still present for the DRY El Niño years but it is replaced by cold SST anomalies for the WET El Niño years. To investigate the time evolution of the SST anomalies during DRY and WET El Niño years, we construct Hovmuller diagrams of the SST and near surface wind composites along the equator (respectively Fig. 3a,b). Not

only are the Pacific SST anomalies warmer in DRY El Niño years, but they also last longer than those in WET El Niño years. In February, the positive SST anomalies disappear near the coast of South America in WET El Niño years. In addition, the maximum SST anomalies occur in the eastern Pacific for the DRY El Niños and in the central Pacific for the WET El Niños. The Pacific subtropical cold anomalies are stronger for the DRY events than the WET events. Thus the meridional SST gradient between the warm tropical anomalies and the cold subtropical anomalies is strongest for the DRY cases. Throughout the paper, strong and long (weak and short) events with maximum SST anomalies in the eastern (central) Pacific as well as strong (weak) meridional SST gradient will be referred to as “long and strong” (“weak and short”) events.

For both DRY and WET cases, SST anomalies are positive in the tropical North Atlantic in DJF (Fig. 2a,b). There, the differences between the two cases are not statistically significant (Fig. 2c). The contrasting SST anomalies in DJF occur in the equatorial and tropical South Atlantic, with weak negative anomalies during DRY El Niño years and strong positive anomalies during WET El Niño years. This explains the weak correlation between NINO3 and SST anomalies in the equatorial and tropical South Atlantic found in previous studies (Zebiak 1993; Enfield and Mayer 1997). The meridional SST gradient in DJF is strongly determined by the tropical South Atlantic with the greatest SST anomaly differences reaching up to 1°C there (Fig. 2c). During the following season (MAM), the SST anomalies are enhanced in both the north and south tropical Atlantic for the DRY El Niño years and damped for the WET El Niño years (Fig. 2d,e respectively). The enhanced warming of the tropical North Atlantic and cooling of the tropical South Atlantic in MAM during DRY El Niño years, establish the positive meridional SST gradient, preventing the ITCZ from moving

southward and reducing precipitation in the NE. The greatest SST anomaly differences occur in the cold tongue and Benguela Current/upwelling regions (Fig. 2f). It is worth mentioning that the equatorial cold tongue develops only during DRY El Niños and earlier in MAM. In neutral years, the Atlantic cold tongue peaks during boreal summer (JJA) (Keenlyside and Latif 2007). Moreover, eastern Atlantic cold (warm) SST anomalies and western Atlantic easterly (westerly) wind anomalies are present as early as November during the DRY (WET) El Niños mature phase (Fig. 3). These coupled anomalies characterize the first element of the Bjerknes feedback. The 1997/98 event is a partial exception to the rule that strong and long El Niño events are generally accompanied by cold SST anomalies in the equatorial and tropical South Atlantic. In this case, there was a warming of the equatorial Atlantic. However, cold anomalies were present at the Benguela upwelling region and the positive anomalies in the tropical North Atlantic were greater than those in the South Atlantic in MAM, therefore the meridional SST gradient was still positive in MAM.

Another important factor to be considered is the existence of a positive phase of the South Atlantic SST dipole mode during WET El Niño years in SON (not shown) and DJF (Fig. 2b). This is the dominant mode of variability in the South Atlantic and is characterized by SST anomalies of opposing signs about a nodal line running approximately along 30°S (Venegas et al. 1997; Sterl and Hazeleger 2003; Haarsma et al. 2003, 2005). The South Atlantic dipole peaks in boreal winter, coinciding with the ENSO mature phase. Haarsma et al. (2003) have shown that the response of the atmosphere to a positive South Atlantic dipole results in a southward displacement of the ITCZ with a weakening of the trades in the western equatorial Atlantic in JFMA (WET El Niño years). Concurrently, during DRY El Niño years there is no apparent South Atlantic dipole mode in DJF, but the SST anomalies show a tripole

pattern in MAM, which resembles the second leading mode of variability in the South Atlantic according to Sterl and Hazeleger (2003).

*b. Atmospheric circulation variability*

We have seen that Pacific and Atlantic SST anomalies vary considerably from one El Niño event to the other. Here we explore the differences in the atmospheric circulation for both types of El Niño identified in the previous section (DRY and WET). In particular, we analyze the main known mechanisms of the tropical ENSO teleconnection: anomalous Walker circulation (the zonal circulation change associated with anomalous zonal displacement of equatorial Pacific convection) and the tropical-extratropical PNA stationary wave.

For DRY El Niño years in JFMA, the Pacific Walker circulation cell is the typical anomalous cell with a reverse sign during the mature phase (Wang 2002a): the air rises in the equatorial eastern Pacific, flows westward aloft, sinks in the equatorial western Pacific, and returns back to the east in the lower troposphere (Fig. 4a). Associated with this anomalous cell is the presence of a lower (upper) tropospheric convergent inflow (divergent outflow) in the equatorial eastern Pacific and a lower (upper) tropospheric divergent outflow (convergent inflow) in the far western Pacific (Fig. 5a,b). Ascending air dominates the central-eastern Pacific east of the date line (Figs. 4a,5c). Anomalous upper-troposphere divergence from the equatorial Pacific to the tropical North Atlantic is consistent with the PNA wave train mechanism.

For WET El Niño years in JFMA, on the other hand, the Walker circulation does not present the reverse sign typical of El Niño years (Fig. 4b). Weak centers of upper-tropospheric divergence and lower-tropospheric convergence are characterized by a weak

upward velocity around the date line (Fig. 5d-f). The atmospheric circulation resembles that from the decay to neutral phases. These results are consistent with the time evolution of the SST anomalies in the Pacific (Fig. 3): the Pacific Walker circulation in JFMA resembles the mature (decay) phase for DRY (WET) El Niños because they are long (short)-lived events.

In the Atlantic for the DRY El Niño years, the center of lower (upper) tropospheric convergence (divergence) over the Amazon migrates northward weakening the upward motion there, which now only occurs west of 70°W along the equator (Figs. 4a,5a-c). The anticipated presence of cold SST anomalies in the ATL3 region (3°N-3°S and 20°W-0°E) in MAM (Fig. 3a) results in a descending motion around 0°E and easterly winds in the western equatorial Atlantic (west of 10°W). The weakening of the upward motion of the Atlantic Walker circulation in the west and the strengthening of the downward motion in the east is consistent with what would only occur later in JJA in neutral years (Wang 2002b). The cooling of the equatorial Atlantic and the warming of the tropical North Atlantic weaken the Hadley circulation in MAM as shown in Fig. 4c. In addition to the weakening there is a northward shift of a few degrees during MAM when the Hadley circulation is normally at its southernmost position. As a consequence there is a deficit of rainfall over the NE.

These results corroborate the discussion in Section 3a (Figs. 2-3). Strong and long El Niño events are generally accompanied by cold SST anomalies over the ATL3 region that produces subsidence there and easterly anomalies in the western equatorial Atlantic, enhancing the typical El Niño response that generates droughts in the NE. For the weak and short-lived WET El Niño years, there is a strong ascending motion associated with warm SST anomalies over the tropical South Atlantic that weakens the Atlantic Walker cell with westerly wind anomalies in the western equatorial Atlantic (Figs. 4b,5d-f). This warming also

strengthens the Hadley circulation and shifts the ITCZ slightly southward (Fig. 4d) bringing more rainfall over the NE.

Another known ENSO teleconnection is the Pacific-South American (PSA) wave train, which is more active from September to November (SON) and corresponds to the second and third leading patterns of circulation variability in the Southern Hemisphere (Karoly 1989; Kiladis and Mo 1998; Mo 2000; Mo and Hakkinen 2001). The second (third) leading PSA pattern is associated with the low-frequency (high-frequency) part of ENSO variability with periods of 40-48 (28-32) months and has its heating source in the eastern (central) Pacific (Rasmusson et al. 1990; Mo 2000; Mo and Hakkinen 2001).

For DRY El Niño years in SON, when the wavelike response is more conspicuous (Vera et al. 2004), the PSA wave train is similar to that described in the literature as typical of El Niño events. This is depicted in the map of eddy streamfunction at 200 hPa (Fig. 6a). The upper troposphere is typically characterized by a pair of anticyclonic (cyclonic) anomalies straddling the equator in the Pacific (Atlantic), the PSA wave train extending from the central equatorial Pacific poleward to South America turning north into the Atlantic, a cyclonic anomaly at the southern tip of South America, and an anticyclonic anomaly over the subtropical South Atlantic, in agreement with Grimm (2003), Vera et al. (2004), and Magaña and Ambrizzi (2005). As expected, this PSA pattern resembles the second leading pattern of ENSO variability, since our DRY cases are longer El Niños with maximum anomalies in the eastern Pacific.

The DRY wave that goes around the tip of South America and into the equatorial Atlantic places an upper-level anticyclonic circulation over the South Atlantic (Fig. 6a). Associated with that, an anomalous anticyclonic circulation develops at lower levels since the

response there is essentially barotropic. This is represented by positive sea level pressure (SLP) anomalies in SON (not shown) and DJF (Fig. 6d) over most of the South Atlantic between  $0^{\circ}\text{S}$  and  $30^{\circ}\text{S}$ . It is associated with an intensification of the South Atlantic subtropical anticyclone, whose center is located around  $30^{\circ}\text{S}$ ,  $5^{\circ}\text{W}$  (Venegas et al. 1997), which leads to easterly wind anomalies in the western equatorial South Atlantic (Fig. 6d). This atmospheric response has a minor impact on the SST anomalies over the South Atlantic, but the easterly anomalies are perhaps partially responsible for cold ATL3 anomalies in OND (Fig. 4a). One could also argue that the easterlies in DJF for the DRY case are caused by the El Niño response in the tropical North Atlantic, however the SLP anomalies are only significantly different in the South Atlantic (Fig. 6f) and the zonal wind anomalies are practically the same in the tropical North Atlantic for both DRY and WET events at this time of the year (Fig. 7).

On the other hand, during WET El Niño years, the pair of anticyclones in the equatorial Pacific is considerably weaker and the cyclonic anomaly at the southern tip of South America is not present (Fig. 6b). The PSA wave train resembles the third leading pattern. This is also corroborated by the results of Silva and Ambrizzi (2006), which show that the PSA pattern of a strong El Niño event (1997/98, DRY case) has a higher amplitude and a more defined wave structure than a weak event (2002/03, WET case). There are two wave paths: one across South America into the equatorial Atlantic and another one around the tip of South America across to South Africa (Fig. 6b). The latter places an upper-level cyclonic circulation over the South Atlantic that leads to the development of an anomalous low-pressure center at  $15^{\circ}\text{S}$ - $50^{\circ}\text{S}$  and  $40^{\circ}\text{W}$ - $10^{\circ}\text{E}$  represented by negative SLP anomalies

(Fig. 6e). This is related to a weakening and north-south displacement of the climatological subtropical high in SON (not shown) and DJF (Fig. 7).

The SST and SLP patterns in DJF are similar to the first leading mode of variability in the South Atlantic (South Atlantic dipole mode) with a SLP monopole centered in  $15^{\circ}\text{W}$ ,  $45^{\circ}\text{S}$  associated with a SST dipole (SST anomalies of opposing signs about a nodal line along  $\sim 30^{\circ}\text{S}$ ). The SLP and SST anomalies for the WET case have the same order of magnitude of those in Sterl and Hazeleger (2003). (Compare our Figs. 2b and 6e with their Fig. 3a.) Over the South Atlantic, the change in the atmospheric circulation caused by the WET PSA wave train is similar to that reported by Sterl and Hazeleger (2003) as being the cause for the establishment of the SST dipole. According to those authors, the SST anomalies are induced by wind anomalies mainly through latent heat flux and vertical mixing in the mixed-layer with minor contribution from Ekman transport. With a simple linearized barotropic model, Hoskins and Ambrizzi (1993) have shown the existence of preferable wave guides associated with the subtropical jets. A local forcing placed at  $90^{\circ}\text{W}$  in the equatorial Pacific generated a wave train similar to our DRY case (compare our Fig. 6a with their Fig. 6b). On the other hand a local source placed at  $105^{\circ}\text{W}$  gave rise to two wave trains over the Atlantic similar to our WET case (compare our Fig. 6b with their Fig. 9a).

The aforementioned observational evidence suggests that the inter-El Niño variability of the NE precipitation is dictated by SST and atmospheric circulation anomalies in the equatorial and tropical South Atlantic. We hypothesize that inter-El Niño variability causes changes in the Walker circulation (direct route) that leads to wind anomalies in the western equatorial Atlantic and SST anomalies in the eastern equatorial and tropical South Atlantic. These SST anomalies determine the meridional SST gradient across the equator, the position

of the ITCZ, and thus the NE precipitation in MAM. The observational results also suggest that inter-El Niño variability of the PSA wave trains (extra-tropical indirect route) cause changes in the atmospheric circulation over the South Atlantic, which in turn can lead to SST anomalies in the tropical South Atlantic in DJF. These SST anomalies can reinforce or hinder the El Niño direct route response in the western tropical Atlantic in MAM.

#### **4. The influence of the Pacific and Atlantic SST variability on the NE precipitation**

Here, we evaluate the quality of the atmospheric circulation simulated by SPEEDY, by comparing SLP, near surface wind, and precipitation from data to those from the DRY and WET runs (SST anomalies prescribed in both the Pacific and Atlantic). We make the comparisons for the period of JFMA, which includes the end of the El Niño mature phase and the beginning of the NE rainy season. SPEEDY reproduces the main features of the ENSO teleconnection for the DRY conditions in JFMA (Fig. 8a,d), namely: the decrease of SLP over the tropical North Atlantic, albeit weaker, as a consequence of an increase in upper-troposphere divergence and a decrease in subsidence there (Section 3b); the presence of easterly anomalies in the western equatorial Atlantic due to the intensification of the Atlantic Walker cell; a weakening and northward shift of the Hadley circulation (not shown); and an intensification of the South Atlantic Subtropical High (positive SLP anomalies over the South Atlantic). For the WET run, SPEEDY reproduces the weakening of the Atlantic Walker cell (westerly anomalies in the western equatorial Atlantic) and of the subtropical high (Fig. 8b,e), as well as a strengthening and southward shift of the Hadley circulation (not shown). Similar to the observations, the statistically significant differences between the DRY and WET El

Niños occur over the equatorial and tropical South Atlantic (Fig. 8c,f). The zonal wind anomaly averaged over 0-10°S and 20-40°W is -0.32 (0.26) m s<sup>-1</sup> from the DRY (WET) run and -0.62 (0.29) m s<sup>-1</sup> from the data in JFMA. The decrease (increase) in the vertical velocity averaged 0-40°W is about 30% (30%) from the DRY (WET) run and 35% (7%) from the data in MAM. Moreover, SPEEDY reproduces the different PSA wave trains in SON (not shown) that lead to the SLP and wind patterns over the South Atlantic.

SPEEDY reproduces reasonably the Atlantic NE precipitation in MAM for DRY and WET conditions (Fig. 9). We find, however, deficient precipitation right over the NE for the WET case. This is due to the fact that the Atlantic ITCZ is generally more to the south in the model than in the data, which is a common deficiency in many AGCMs (Biasutti et al. 2006). The ITCZ is already to the south of its general observed position for the climatological run. The WET case tends to push the ITCZ even further to the south causing negative anomalies over the NE. The observed NE precipitation is highly correlated to the precipitation over the adjacent oceanic area between 0-15°S and 0-50°W. SPEEDY reproduces the correct sign of the precipitation over this area. The anomalous precipitation reaches -3.3 (2.5) mm day<sup>-1</sup> in the model and -4.1 (3.1) mm day<sup>-1</sup> in the data for the DRY (WET) case. Thus we consider precipitation averaged over this area in our estimates throughout the manuscript.

To investigate the sensitivity of the NE precipitation to the direct influence of each basin separately, we designed 8 extra experiments with prescribed SST anomalies only in: the Pacific, the Atlantic, the North Atlantic, and the South Atlantic for both DRY and WET conditions. Climatological SST is prescribed elsewhere. Fig. 10 shows DRY minus WET NE precipitation anomalies for each basin. The Atlantic SST anomalies play an overwhelming role on the NE precipitation when compared to the Pacific SST anomalies (see Fig. 9f and

Fig. 10a,b). This is somehow expected and corroborates findings from previous studies (Pezzi and Cavalcanti 2001; Giannini et al. 2004, Barreiro et al. 2005). In particular, Misra (2006; 2007) have highlighted the importance of coupled air-sea interaction in determining NE precipitation. Though the main point revealed here (Fig. 10c,d) is that the equatorial and tropical South Atlantic, and not the tropical North Atlantic, plays a more important role on the NE precipitation during El Niño years, confirming the observational evidences shown in the previous section. The DRY-WET precipitation pattern for the South Atlantic run is almost identical to that for the Atlantic run, with little contribution from the North Atlantic. Moreover, changes in the Hadley circulation are very sensitive to the South Atlantic SST anomalies (compare Fig. 10e and 10f).

## **5. Equatorial and tropical South Atlantic SST variability predetermined by the El Niño events**

It is well known that a great part of the SST anomalies in the tropical North Atlantic during El Niño events is generated by the ENSO teleconnection (Enfield and Mayer 1997, Hastenrath 2006, among others). However, the systematic occurrence of cold anomalies in the equatorial and tropical South Atlantic in MAM during long and strong El Niño events versus warm anomalies during short and weak El Niños events suggests that the SST anomalies in the equatorial and tropical South Atlantic might be predetermined by the El Niño as well. Here we examine the results from SPEEDY coupled to a slab ocean model and to MICOM, in which the Atlantic basin is allowed to respond to changes in the atmospheric circulation caused by inter-El Niño variability.

For the DRY El Niño case, both SLAB and MICOM runs simulate a cooling in the equatorial and tropical South Atlantic during the NE rainy season MAM (Fig. 11a,d, respectively). However, the SLAB run does not reproduce properly the location and extent of the cooling when compared to the observations (Fig. 2d). For the WET El Niño case, the SLAB run simulates a cooling in the central tropical Atlantic whereas the MICOM run reproduces well the widespread warming in the tropical South Atlantic, which is similar to the observations (compare Figs. 11b,d and 2e).

Only MICOM is able to reproduce the correct evolution of the SST anomalies in the South Atlantic between the equator and 30°S (Fig. 12). Note that the SST anomaly differences between DRY and WET cases are only statistically significant from November onwards in both observations and MICOM. As discussed in Section 3b, the intensification of the South Atlantic subtropical anticyclone for the DRY run and of the southerly trades generates cold anomalies from November on. For the WET run, the weakening of the South Atlantic subtropical high and of the southerly trades leads to the warming of the tropical South Atlantic (equatorward pole of the South Atlantic dipole mode). The most prominent atmospheric response to this warming consists of an anomalous low-pressure system centered at approximately 20°W, 30°S in austral summer (Fig 8k). This response is similar to the deep baroclinic response obtained by Robertson et al. (2003) and Haarsma et al. (2003). The SLAB run fails in reproducing the atmospheric changes in JFMA (Fig. 8h) that leads to the correct SST and precipitation anomalies in MAM (see next section).

A close analysis of the heat flux components for the SLAB run shows that the cooling in the South Atlantic is driven by the latent heat loss (not shown). The increase in the southerly trade winds and the strengthening of the South Atlantic subtropical high (Fig. 8g)

induces the wind-evaporation-SST (WES) feedback (Xie and Philander 1994) that leads to the cooling in the western side of the basin. For this reason, there is a warming in the eastern equatorial Atlantic and a cooling in the western-central equatorial and tropical South Atlantic (Fig. 11a) contrary to the observations (Fig. 2d).

On the other hand, MICOM reproduces the cooling in the eastern equatorial Atlantic and Benguela upwelling in DJF (not shown), MAM (Fig. 11d), and JJA (not shown) for the DRY run. One piece of evidence that ocean dynamics is essential in generating the SST anomalies in MAM comes from the analysis of the net surface heat flux (Fig. 13a). For most regions in the equatorial and tropical South Atlantic the sign of the SST anomalies opposes that of the net surface heat flux. We can conclude that the atmosphere opposes the changes in the mixed layer temperature and that they are generated by ocean heat transport (this will be discussed in detail below).

Therefore, only the MICOM runs are capable of reproducing the correct meridional SST gradient in MAM that dictates the position of the ITCZ and the NE precipitation (Fig. 9g-l). Even though the ITCZ simulated by SPEEDY is to the south of the observed ITCZ, the precipitation over 0-15°S and 0-50°W reaches up to -4.1 and 1.8 mm day<sup>-1</sup> for the DRY and WET MICOM runs, respectively. Whereas for the SLAB runs, anomalous precipitation has the same sign for both DRY and WET runs, -4.3 and -3.3 mm day<sup>-1</sup>, respectively.

#### *a. The crucial role of ocean dynamics*

During El Niño years, the cold (warm) events in the equatorial Atlantic in MAM are associated with anomalous easterlies (westerlies) in the western tropical Atlantic in JFMA (Fig. 8j,k) and are achieved mainly by means of the Bjerknes feedback (Chang et al. 2006).

According to Keenlyside and Latif (2007), the Bjerknes mechanism is active mainly during boreal summer (JJA). Comparing to neutral years, DRY El Niño events seem to anticipate the cold tongue mode in both observations and MICOM results. The wind changes, remotely caused by the ENSO teleconnection, lead to an earlier cooling in the eastern equatorial Atlantic in MAM. This establishes a positive meridional SST gradient that prevents the ITCZ from moving southward in MAM causing droughts in the NE. The eastern equatorial cooling in turn enhances the wind in the western equatorial basin that causes further cooling in the eastern equatorial basin in JJA (locally generated). For the WET El Niño events, the cold tongue does not develop in MAM and JJA as a consequence of westerly anomalies. Thus, the ITCZ is allowed to move southward bringing rainfall to the NE.

The strong relationship between the eastern equatorial Atlantic SST anomalies and the western Atlantic zonal winds represents only the first element of the Bjerknes feedback (Keenlyside and Latif 2007). The second element involves the link between western Atlantic zonal winds and eastern Atlantic thermocline depth (Fig. 13d-f). The easterly anomalies are associated with a decrease (an increase) of the thermocline depth in the eastern (western) equatorial Atlantic in MAM for the DRY run. For the WET run, the thermocline is practically flat along the equator. The third element of the Bjerknes feedback is the coupling between ocean dynamics and SST variability and the dominant term in this coupling is the mean vertical advection of temperature (Neelin et al. 1998). The main contribution to the cooling of the eastern Atlantic is due to the increase in vertical entrainment for the DRY run (negative values in Fig. 13g). For the WET run, the warming is associated with a reduction of entrainment along the equator (Fig. 13h).

The wind anomalies in the western equatorial Atlantic are also responsible for creating SST anomalies in the Benguela Current/upwelling region. Florenchie et al. (2003, 2004) have shown that Benguela Niños, which peak in March and April, are remotely generated by wind anomalies in the equatorial west-central Atlantic in January. These wind anomalies generally trigger Kelvin waves that propagate eastward along the equator reaching the African coast and inducing coastal-trapped waves that propagate southward. Shallower (deeper) thermocline and enhanced (reduced) entrainment are present off the coast of Africa mainly south of  $15^{\circ}\text{S}$  for the DRY (WET) run (Fig. 13d-i). Since the SLAB run does not contain ocean dynamics, it is incapable of simulating the cooling in the eastern equatorial Atlantic and Benguela upwelling.

Besides the eastern part of the basin, there is another region in the South Atlantic where ocean dynamics seems to play a role. According to Foltz and McPhaden (2006), the horizontal oceanic heat advection is responsible for damping the surface-flux-forced changes in SST mainly between  $0\text{-}35^{\circ}\text{W}$  and  $10\text{-}20^{\circ}\text{S}$ . In this region, the MICOM run presents a warming in DJF and MAM (the middle pole of the South Atlantic SST tripole pattern) in agreement with the observations (compare Fig. 11d and Fig. 2d). This is also absent in the SLAB run (Fig. 11a).

Finally, SST changes in the equatorial and south tropical Atlantic due to the ocean dynamics have an indirect impact over the tropical North Atlantic, where surface heat flux is supposed to drive the SST changes. In both SLAB and MICOM runs, the tropical North Atlantic presents a warming for the DRY and WET runs in DJF (not shown) and MAM (Fig. 11). This is consistent with the typical ENSO atmospheric bridge, i.e., PNA wave and tropospheric warming mechanisms. Contrary to the South Atlantic, the net surface heat flux

and the mixed-layer SST anomalies have the same sign in the tropical North Atlantic for both DRY and WET runs in DJF (not shown) and MAM (Figs. 13a,b and 2a,b, respectively), suggesting that they are generated by the atmosphere. According to Lee et al. (2008), only long El Niño events (our DRY case) cause a further warming in MAM in the tropical North Atlantic. Our results (Fig. 11) corroborate Lee et al. (2008) findings. However, only in the MICOM run (Fig. 11d-f), is this warming (DRY case) statistically significantly different from that caused by the short El Niños (WET case). For the DRY case, the cooling of the equatorial Atlantic weakens the Hadley circulation (not shown) decreasing even further the northeastern trades (compare Fig. 8g and 8j). For the WET case, the warming of the equatorial Atlantic enhances the Hadley circulation counteracting the reduction in the northeastern trades, particularly in the eastern tropical North Atlantic. This explains why short-lived El Niños (WET) do not warm up as much as the long-lived ones (DRY). Note that the results from Section 4 have shown that changes in the Hadley circulation are more sensitive to the equatorial and tropical South Atlantic SST anomalies than the tropical North Atlantic SST anomalies (Fig. 10e,f). Moreover, if the further warming of the tropical North Atlantic is caused exclusively by the WES feedback, it should have been reproduced satisfactorily in the DRY SLAB run (Fig. 11b).

## **6. Summary and Conclusions**

In this study, we have identified from data analysis different SST patterns in both the Pacific and Atlantic oceans during El Niño years that lead to NE precipitation below and above the average in MAM: 1) DRY (WET) NE cases are related to strong and long (weak and short) El Niño events that have the strongest warming in the eastern (central) Pacific; 2)

strong and long (weak and short) El Niño events are associated with cold (warm) anomalies in the equatorial Atlantic and Benguela Current region in DJF, MAM, and JJA; 3) the contrasting SST anomalies between the DRY and WET cases that establish the sign of the meridional SST gradient in MAM are found in the equatorial and tropical South Atlantic; 4) the South Atlantic dipole mode develops in SON/DJF only during weak and short El Niño events (WET) and the cold tongue develops in MAM /JJA only during strong and long El Niño events (DRY).

Previous studies did not find significant correlations between NINO3.4 and the tropical-subtropical South Atlantic because half of the El Niño events during the period generally considered (1950-2000) caused one atmospheric-SST response (anticyclonic and cold anomalies) and the other half caused the opposite response (cyclonic and warm anomalies) (Barreiro et al. 2004, 2005 and Giannini et al. 2004 among others). If inter-event variability is not considered, significant correlations will not be found over the equatorial and tropical South Atlantic. These non-significant correlations led to the conclusion that the South Atlantic variability was independent of the ENSO. On the other hand, since the response in the tropical North Atlantic is very similar for all El Niño events, the correlation between NINO3.4 and SST anomalies in the tropical North Atlantic is positive and statistically significant. Consequently, it was previously thought that only the tropical North Atlantic responds to El Niño (or ENSO). At the time these studies were developed, only La Niña versus El Niño responses were considered. It is necessary to go one step forward, or one level up into the different El Niño events to realize that El Niño plays an important role in establishing the SST anomalies in the South Atlantic.

From numerical simulations, we have shown that the preexistent SST anomalies in the equatorial and tropical South Atlantic in DJF/MAM are crucial in determining the NE precipitation in MAM and that they are determined by the inter-El Niño variability through ocean dynamics. Strong and long (weak and short) El Niños with a heating source in the eastern (central) Pacific trigger the second (third) leading PSA pattern in SON, which in turn causes among other things a strengthening (weakening) of the South Atlantic subtropical high.

For the DRY events, the strengthening of the subtropical high is associated with an increase in the southerly trades with negative SST anomalies in the equatorial Atlantic in November and December when the Bjerknes mechanism is active for the second time in the year (Okumura and Xie 2006). This is an indirect extra-tropical atmospheric route that together with changes in the Walker circulation (direct tropical route) in JFMA leads to the development of the cold tongue (Bjerknes mechanism) and Benguela upwelling in MAM. A positive meridional SST gradient is established in MAM preventing the southward movement of the ITCZ causing a rainfall deficit over the NE.

For the WET events, the weakening of the subtropical high sets the South Atlantic dipole with warm SST anomalies in the tropical South Atlantic in DJF, that in turn hinders the effects of the direct ENSO teleconnection. As a consequence the ITCZ is allowed to move southward bringing rain to the NE. The seasonal phase locking between the mature phase of El Niño (NDJ), wind stress anomalies (JFMA) due to changes in the Walker cell (caused by both direct and indirect routes), and the oceanic response in the equatorial and tropical South Atlantic (MAM) is fundamental in establishing the precipitation anomalies in the NE (MAM). Our results highlight the importance of ocean dynamics on the NE climate. Only coupled SPEEDY-MICOM runs were able to simulate the correct SST anomalies in the Atlantic.

Chang et al. (2006) have also found that El Niño years with easterly wind anomalies in the western equatorial Atlantic were associated with cold anomalies in the eastern equatorial Atlantic and that El Niño years with westerly wind anomalies (or weak easterly anomalies) were associated with warm anomalies in the equatorial Atlantic. They showed that in spite of having similar tropospheric warming, only El Niño events with westerlies in the equatorial Atlantic would lead to a warming of the equatorial and tropical Atlantic. The El Niño years with easterlies developed the cold tongue “destroying” the El Niño response. There is one caveat to this conclusion, which is to expect that 1) the tropospheric warming is the main ENSO teleconnection mechanism and 2) consequently El Niños cause warming of the equatorial and tropical South Atlantic. This might be the case for the tropical North Atlantic, where a decrease in the SLP leads to a weakening of the trades and the warming of the tropical North Atlantic by means of WES mechanism.

These results are important to improve our capability of predicting the climate of the NE. The presence of zonal wind anomalies in the western equatorial Atlantic in DJF is crucial for the development of equatorial and tropical South Atlantic SST anomalies that establish the sign of the meridional SST gradient in MAM and the NE precipitation. Thus these wind anomalies in DJF are a good predictor of the NE precipitation in MAM. They are also highly correlated to the Pacific-Atlantic thermal gradient (NINO3-ATL3), with a correlation coefficient of -0.8 during El Niño years. To illustrate the importance of the Pacific-Atlantic thermal gradient over the meridional SST gradient (given by the DIPOLE index) in DJF, a simple multiple regression model was used to predict the NE precipitation in MAM (Table 1). The correlation between the observed precipitation and that predicted using only DJF DIPOLE is 0.64 and using DJF NINO3-ATL3 is 0.81. Using both, the correlation is 0.83,

which is not significantly different from the correlation using NINO3-ATL3 alone. Thus the simple NINO3-ATL3 index in DJF could be used as a predictor of the NE precipitation in MAM. The central role of ocean dynamics is indirectly represented by this index.

This study is also relevant to the climate of southern South America and western Africa. ENSO generally causes a dipole-like pattern of the precipitation over South America: dry (wet) conditions over the northeast are associated with wet (dry) conditions over southeast South America (Grimm 2003). The meridional excursion of the ITCZ also affects the precipitation over the sub-Saharan. In El Niño years that the cold tongue does not develop in MAM/JJA and the equatorial Atlantic presents warm anomalies, the ITCZ tends to stay in its southernmost position leading to wet conditions over the NE and dry conditions over the sub-Saharan. An anticorrelation between the precipitation over the two regions has already been found in previous studies (Hastenrath 1995; Rao et al. 2006).

Finally, a set of idealized numerical experiments is under way to determine which characteristics of the El Niño event are more relevant to establish the correct Atlantic meridional SST gradient in MAM. The likely candidates are: position of the heating source, magnitude of the heating, time evolution of the event, and the meridional gradient between warm anomalies in the equatorial Pacific and the cold anomalies in the subtropical south-central Pacific. We believe that the location of the heating source plays an important role in determining the type of PSA (indirect route) and consequent response over the South Atlantic earlier on, in SON-DJF (Kao and Yu 2009; Kumar et al. 2006; Magaña and Ambrizzi 2005). Though the study by Vera et al. (2004) shows that the meridional SST gradient between the warm tropical anomalies and the cold subtropical anomalies in the Pacific is also important in determining the PSA pattern. It might be a combination of the two characteristics since

generally the eastern (central) Pacific events have the strong (weaker) meridional SST gradient. The preconditioning of the Atlantic SST, caused by the PSA, is the most important factor for the NE precipitation because it will enhance or weaken the direct route El Niño teleconnection (corroborated by Barreiro et al. 2004 and 2005). However, the amplitude of the warming seems to be important for the direct route in terms of changes in the stability of the atmospheric column (tropospheric warming, Chiang and Lintner 2005 and Chang et al. 2006). Finally, another characteristic is the time evolution. Lee et al. (2008) have shown that longer El Niños cause a stronger warming of the tropical North Atlantic.

*Acknowledgments.*

We would like to thank Camiel Severijns and Douglas Vieira for helping with the model simulations. The authors thank the two anonymous reviewers for their valuable contribution. RRR especially thanks FAPESP for support (Grants 2007/03279-5 and 2008/01565-3). EJDC and TA thank the partial support of CNPq. This work was partially funded by the IAI (Grants CRNII-047, CRNII-076, and NSF Grant GEO-0452325). ECMWF ERA-40 data used in this study was obtained from the ECMWF data server.

## References

- Adler, R. F., and Coauthors, 2003: The version 2 Global Precipitation Climatology Project (GPCP) monthly precipitation analysis (1979-present). *J. Hydrometeor.*, **4**, 1147-1167.
- Barreiro, M., A. Giannini, P. Chang, and R. Saravanan, 2004: On the role of the South Atlantic atmospheric circulation in tropical Atlantic variability. *Earth's Climate: The Ocean-Atmosphere Interaction, Geophys. Monogr.*, Vol. 147, Amer. Geophys. Union, 143–152.
- Barreiro, M., P. Chang, L. Ji, R. Saravanan, and A. Giannini, 2005: Dynamical elements of predicting boreal spring tropical Atlantic sea-surface temperatures. *Dyn. Atmos. Oceans*, **39**, 61-85.
- Biasutti, M., A. H. Sobel, and Y. Kushnir, 2006: AGCM precipitation biases in the tropical Atlantic. *J. Climate*, **19**, 935-958.
- Chang, P., Y. Fang, R. Saravanan, L. Ji, and H. Seidel, 2006: The cause of the fragile relationship between the Pacific El Niño and the Atlantic Niño. *Nature*, **443**, 324-328.
- Chiang, J. C. H., and B. R. Lintner, 2005: Mechanisms of remote tropical surface warming during El Niño. *J. Climate*, **18**, 4130-4149.
- Enfield, D.B., and D. A. Mayer, 1997: Tropical Atlantic sea surface temperature variability and its relation to El Niño-Southern Oscillation. *J. Geophys. Res.*, **102**, 929-945.
- Florenchie, P., J. R. E. Lutjeharms, C. J. C. Reason, S. Masson, and M. Rouault, 2003: The source of Benguela Niños in the South Atlantic Ocean. *Geophys. Res. Lett.*, **30**, doi:10.1029/2006GL017172.

- Florenchie, P., C. J. C. Reason, J. R. E. Lutjeharms, M. Rouault, C. Roy, and S. Masson, 2004: Evolution of interannual warm and cold events in the Southeast Atlantic Ocean. *J. Climate*, **17**, 2318-2334.
- Foltz, G. R., and M. J. McPhaden, 2006: The role of oceanic heat advection in the evolution of tropical North and South Atlantic SST anomalies. *J. Climate*, **19**, 6122-6138.
- Giannini, A., R. Saravanan, and P. Chang, 2004: The preconditioning role of Tropical Atlantic Variability in the development of the ENSO teleconnection: implications for the prediction of Nordeste rainfall. *Climate Dyn.*, **22**, 839-855.
- Grimm, A. M., 2003: The El Niño impact on the summer monsoon in Brazil: Regional processes versus remote influences. *J. Climate*, **16**, 263-280.
- Grimm, A. M., and T. Ambrizzi, 2009: Teleconnections into South America from the tropics and extratropics on interannual and intraseasonal timescales. *Past Climate Variability in South America and Surrounding Regions*, F. Vimeux, F. Sylvestre, and M. Khodri, Eds., Springer, 159-191.
- Grimm, A. M., and R. Tedeschi, 2009: ENSO and extreme rainfall events in South America. *J. Climate*, **22**, 1589-1609.
- Haarsma, R. J., E. J. D. Campos, and F. Molteni, 2003: Atmospheric response to South Atlantic SST dipole. *Geophys. Res. Lett.*, **30**, doi:10.1029/2003GL017829.
- Haarsma, R. J., E. J. D. Campos, W. Hazeleger, C. Severijns, A. R. Piola, and F. Molteni, 2005: Dominant modes of variability in the South Atlantic: A study with a hierarchy of ocean-atmosphere models. *J. Climate*, **18**, 1719-1735.

- Hastenrath, S., 1995: Recent advances in tropical climate prediction. *J. Climate*, **8**, 1519-1532.
- Hastenrath, S., 2006: Circulation and teleconnection mechanisms of Northeast Brazil droughts. *Prog. Oceanogr.*, **70**, 407-415.
- Hastenrath, S., and L. Heller, 1977: Dynamics Of Climatic Hazards In Northeast Brazil. *Quart. J. Roy. Meteor. Soc.*, **103**, 77-92.
- Hazeleger, W., and R. J. Haarsma, 2005: Sensitivity of tropical Atlantic climate to mixing in a coupled ocean-atmosphere model. *Climate Dyn.*, **25**, 387-399.
- Hoskins, B. J., and T. Ambrizzi, 1993: Wave propagation on a realistic longitudinally varying flow. *J. Atmos. Sci.*, **50**, 1661-1671.
- Kao, H.-Y., and J.-Y. Yu, 2009: Contrasting eastern-Pacific and central-Pacific types of El Niño. *J. Climate*, **22**, 615-632.
- Karoly, D. J., 1989: Southern Hemisphere circulation features associated with El Niño-Southern Oscillation events. *J. Climate*, **2**, 1239-1251.
- Keenlyside, N. S., and M. Latif, 2007: Understanding equatorial Atlantic interannual variability. *J. Climate*, **20**, 131-142.
- Kiladis, G. N., and K. C. Mo, 1998: Interannual and intraseasonal variability in the Southern Hemisphere. *Meteorology of the Southern Hemisphere*, D. J. Karoly and D. G. Vincent, Eds., Amer. Meteor. Soc., 307-336.
- Kumar, K. K., B. Rajagopalan, M. Hoerling, G. Bates, and M. Cane, 2006: Unraveling the mystery of Indian monsoon failure during El Niño. *Science*, **314**, 115-119.

- Lee, S.-K., D. B. Enfield, and C. Wang, 2008: Why do some El Niños have no impact on tropical North Atlantic SST? *Geophys. Res. Lett.*, **35**, doi:10.1029/2008GL034734.
- Magaña, V., and T. Ambrizzi, 2005: Dynamics of subtropical vertical motions over the Americas during El Niño boreal winters. *Atmósfera*, **18**, 211-235.
- Misra, V., 2006: Understanding the predictability of seasonal precipitation over northeast Brazil. *Tellus*, **58**, 307-319.
- Misra, V., 2007: A Sensitivity study of the coupled simulation of the Northeast Brazil rainfall variability. *J. Geophys. Res.*, **112**, D11111, doi:10.1029/2006JD008093.
- Mo, K. C., 2000: Relationship between low-frequency variability in the Southern Hemisphere and sea surface temperature anomalies. *J. Climate*, **13**, 3599-3610.
- Mo, K. C., and S. Hakkinen, 2001: Decadal variations in the tropical South Atlantic and linkages to the Pacific. *Geophys. Res. Lett.*, **28**, 2065-2068.
- Molteni, F., 2003: Atmospheric simulations using a GCM with simplified physical parameterization. I: Model climatology and variability in multi-decadal experiments. *Climate Dyn.*, **20**, 175-191.
- Moura, A. D., and J. Shukla, 1981: On the dynamics of droughts In northeast Brazil - Observations, theory and numerical experiments with a general-circulation model. *J. Atmos. Sci.*, **38**, 2653-2675.
- Neelin, J. D., D. S. Battisti, A. C. Hirst, F.-F. Jin, Y. Wakata, T. Yamagata, and S. E. Zebiak, 1998: ENSO theory. *J. Geophys. Res.*, **103**, 14 261-14 290.
- Nobre, P., and J. Shukla, 1996: Variations of Sea Surface Temperature, Wind Stress, and Rainfall over the Tropical Atlantic and South America. *J. Climate*, **9**, 2464-2479.

- Okumura, Y., and S.-P. Xie, 2006: Some overlooked features of tropical Atlantic climate leading to a new Niño-like phenomenon. *J. Climate*, **19**, 5859-5874.
- Pezzi, L. P., and I. F. A. Cavalcanti, 2001: The relative importance of ENSO and tropical Atlantic sea surface temperature anomalies for seasonal precipitation over South America: a numerical study. *Climate Dyn.*, **17**, 205-212.
- Rao, V. B., E. Giarolla, M. T. Kayano, and S. H. Franchito, 2006: Is the recent increasing trend of rainfall over northeast Brazil related to sub-Saharan drought? *J. Climate*, **19**, 4448-4453.
- Rasmusson, E. M., X. Wang, C. F. Ropelewski, 1990: The biennial component of ENSO variability. *J. Mar. Syst.*, **1**, 71-96.
- Reason, C. J. C., and D. Jagadheesha, 2005: A model investigation of recent ENSO impacts over southern Africa. *Meteorol. Atmos. Phys.*, **89**, 181-205.
- Robertson, A. W., J. D. Farrara, and C. R. Mechoso, 2003: Simulations of the atmospheric response to South Atlantic sea surface temperature anomalies. *J. Climate*, **16**, 2540-2551.
- Silva, G. M., and T. Ambrizzi, 2006: Inter-El Niño variability and its impacts on the South American low-level jet east of the Andes during austral summer – two case studies. *Advances in Geosci.*, **6**, 283-286.
- Smith, T. M., and R. W. Reynolds, 2004: Improved extended reconstruction of SST (1854-1997). *J. Climate*, **17**, 2466-2477.
- Sterl, A., and W. Hazeleger, 2003: Coupled variability and air-sea interaction in the South Atlantic Ocean. *Climate Dyn.*, **21**, 559-571.

- Taschetto, A. S., C. C. Ummenhofer, A. Sen Gupta, and M. H. England, 2009: The effect of anomalous warming in the central Pacific on the Australian monsoon. *Geophys. Res. Lett.*, **36**, doi:10.1029/2009GL038416.
- Trenberth, K. E., 1997: The definition of El Niño. *Bull. Amer. Meteor. Soc.*, **78**, 2771-2777.
- Venegas, S. A., L. A. Mysak, and D. N. Straub, 1997: Atmosphere-Ocean coupled variability in the South Atlantic. *J. Climate*, **10**, 2904-2920.
- Vera, C., G. Silvestre, V. Barros, A. Carril, 2004: Differences in El Niño response over the Southern Hemisphere. *J. Climate*, **17**, 1741-1753
- Wang, C., 2002a: Atmospheric circulation cells associated with the El Niño-Southern Oscillation. *J. Climate*, **15**, 399-419.
- Wang, C., 2002b: Atlantic climate variability and its associated atmospheric circulation cells. *J. Climate*, **15**, 1516-1536.
- Wang, G., and H. H. Hendon, 2007: Sensitivity of Australian rainfall to inter-El Niño variations. *J. Climate*, **20**, 4211-4226.
- Xie, S. P., and S. G. H. Philander, 1994: A coupled ocean-atmosphere model of relevance to the ITCZ in the eastern Pacific. *Tellus*, **46**, 340-350.
- Zebiak, S. E., 1993: Air-sea interaction in the equatorial Atlantic region. *J. Climate*, **6**, 1567-1586.

## List of Figures

FIG. 1. (a) Precipitation averaged over March-May (MAM) estimated from GPCP dataset (solid line) and FUNCEME dataset (dashed line) for 1979-2005. (b) Scatterplot of NINO3 index (boreal winter, DJF) and NE precipitation from FUNCEME (boreal spring, MAM). Anomalies are normalized by their standard deviations ( $0.93^{\circ}\text{C}$  and  $60\text{ mm}$ , respectively). Asterisks represent non El Niño years. Moderate to extreme El Niño are represented by triangles (circles) when precipitation is below (above) the average. Note that they are labeled by the year corresponding to December of the onset year. Top corner shows area over which precipitation was estimated: solid box for the GPCP dataset and dashed line for the FUNCEME dataset.

FIG. 2. Composites of SST anomaly ( $^{\circ}\text{C}$ ) in DJF for El Niño years in which the precipitation over the NE is (a) below the average (“DRY”) and (b) above the average (“WET”) for the period of 1957-2002. (c) DRY minus WET composites of SST anomalies in DJF. (d), (e), and (f) same as (a), (b), and (c), except for MAM. Solid and dashed lines in (c) and (f) encompass areas where the difference between the means of the anomalies in DRY and WET El Niño years are statistically significant at 99% and 95% confidence levels, respectively.

FIG. 3. Hovmuller diagrams of SST anomalies (contours, in  $^{\circ}\text{C}$ ) and near surface wind anomalies (arrows, in  $\text{m s}^{-1}$ ) averaged between  $2.5^{\circ}\text{S}$  and  $2.5^{\circ}\text{N}$  for 1957-2002: (a) composite of DRY El Niño years; (b) composite of WET El Niño years. The contour interval is  $0.2^{\circ}\text{C}$ . Thick solid lines represent zero contours. Shading indicates where the difference between the means of the anomalies in DRY and WET El Niño years are statistically significant at 95% confidence level. Months within the rectangle represent the El Niño mature phase (NDJF) and subsequent rainy season in the NE (MAM).

FIG. 4. Walker circulation anomalies by averaging zonal divergent wind and vertical velocity anomalies between 2°S and 2°N for JFMA ( $\text{m s}^{-1}$ ,  $\text{hPa s}^{-1}$ ): (a) composite of DRY El Niño years; (b) composite of WET El Niño years. Hadley circulation anomalies by averaging vertical velocity between 50°W and 0°E for MAM ( $\text{hPa s}^{-1}$ ): (c) composite of DRY El Niño years; (d) composite of WET El Niño years. The contour interval is  $0.5 \text{ hPa s}^{-1}$ . Dashed lines indicate negative values (upward motion). The zero contour is omitted.

FIG. 5. Composites for DRY El Niño years in JFMA: (a) 200-hPa velocity potential anomalies ( $10^6 \text{ m}^2 \text{ s}^{-1}$ ) and divergent wind anomalies ( $\text{m s}^{-1}$ ); (b) 850 hPa velocity potential anomalies ( $10^6 \text{ m}^2 \text{ s}^{-1}$ ) and divergent wind anomalies ( $\text{m s}^{-1}$ ); (c) 500-hPa vertical velocity anomalies ( $\text{hPa s}^{-1}$ ). (d), (e), and (f) same as (a), (b), and (c) except for WET El Niño years. The contour interval is  $0.5 \times 10^6 \text{ m}^2 \text{ s}^{-1}$  for (a), (b), (d), (e) and  $1 \text{ hPa s}^{-1}$  for (c), (f). Thick solid lines represent zero contours. Shading indicates where the difference between the means of the anomalies in DRY and WET El Niño years are statistically significant at 95% confidence level.

FIG. 6. Composites of eddy streamfunction at 200 hPa ( $10^6 \text{ m}^2 \text{ s}^{-1}$ ) in SON for (a) DRY, (b) WET, and (c) DRY minus WET. (d), (e), and (f) same as (a), (b), and (c), except for sea level pressure (contours, in hPa) and near surface wind (vectors, in  $\text{m s}^{-1}$ ) in DJF. Solid and dashed lines in (c) and (f) encompass areas where the difference between the means of the anomalies in DRY and WET El Niño years are statistically significant at 99% and 95% confidence levels, respectively.

FIG. 7. Zonal wind zonally averaged over the Atlantic between 40°W and 0°E: DJF climatology (solid line), DRY El Niño years (dashed line), and WET El Niño years (dotted line).

FIG. 8. Sea level pressure (contours, hPa) and near surface wind (vectors,  $\text{m s}^{-1}$ ) in JFMA from observations (a) composites for DRY El Nino years, (b) composites for WET El Nino years, (c) DRY-WET; from the prescribed SST model run (d) DRY run, (e) WET run, (f) DRY-WET runs. (g), (h), (i) and (j), (k), (l) same as (d), (e), (f), except for SLAB and MICOM runs, respectively. Solid and dashed lines encompass the regions where the differences between DRY and WET composites are statistically significant at the 99% and 95% confidence level.

FIG. 9. Same as Fig. 8, except for precipitation ( $\text{mm day}^{-1}$ ) in MAM. The contour interval is  $0.5 \text{ mm day}^{-1}$ . Shown in (c), (f), (i), and (l) contours where the differences are statistically significant at the 95% confidence level.

FIG. 10. Precipitation ( $\text{mm day}^{-1}$ ) in MAM from the DRY minus WET runs where the SST anomalies were prescribed only in: (a) Pacific, (b) Atlantic, (c) North Atlantic, and (d) South Atlantic. The contour interval is  $0.5 \text{ mm day}^{-1}$ . (e), (f) same as (c), (d) except for vertical velocity averaged over  $50^{\circ}\text{W}-0^{\circ}\text{E}$  for MAM ( $\text{hPa s}^{-1}$ ). The contour interval is  $0.2 \text{ hPa s}^{-1}$ . Dashed lines indicate negative values (upward motion). The zero contour is omitted.

FIG. 11. SST anomalies in MAM from SPEEDY-SLAB: (a) DRY run, (b) WET run, (c) DRY-WET runs; and from SPEEDY-MICOM: (c) DRY run, (d) WET run, (e) DRY-WET runs. Solid and dashed lines encompass the regions where the differences between DRY and WET runs are statistically significant at the 99% and 95% confidence level.

FIG. 12. Hovmuller diagrams of SST anomalies (contours, in  $^{\circ}\text{C}$ ) averaged between  $30^{\circ}\text{S}$  and  $0^{\circ}\text{N}$  from observation: composite of (a) DRY and (b) WET El Niño years; from the SLAB (c) DRY and (d) WET runs; from the MICOM (e) DRY and (f) WET runs. The contour interval is  $0.1^{\circ}\text{C}$ . Thick solid lines represent zero contours. Shading indicates where the difference

between the means of the anomalies in DRY and WET El Niño years are statistically significant at 95% confidence level. Months within the rectangle represent the El Niño mature phase (NDJF) and subsequent rainy season in the NE (MAM).

FIG. 13. Net surface heat flux ( $\text{W m}^{-2}$ ) in MAM from the SPEEDY-MICOM: (a) DRY run (b) WET run, and (c) DRY-WET runs. (d), (e), (f) and (g), (h), (i) same as (a), (b), (c), except for depth of the  $20^\circ\text{C}$  isotherm (m) and vertical heat transport ( $\text{K s}^{-1}$ ), respectively. Solid and dashed lines encompass the regions where the differences between DRY and WET runs are statistically significant at the 99% and 95% confidence level.

TABLE 1. Correlation coefficients between observed precipitation over the NE in MAM and: 1) precipitation predicted by the multiple linear regression model using NINO3-ATL3 and DIPOLE in DJF, 2) precipitation predicted by NINO3-ATL3 alone in DJF, 3) precipitation predicted by DIPOLE alone in DJF. NINO3 is SST anomalies averaged over 5°N-5°S and 150°W-90°W; ATL3 is SST anomalies averaged over 3°N-3°S and 20°W-0°E; DIPOLE is SST anomalies averaged over the tropical North Atlantic (5°N-28°N, 60°W-20°W) minus those averaged over the tropical South Atlantic (20°S-5°N, 30°W-10°E).

	NINO3-ATL3 + DIPOLE	NINO3-ATL3	DIPOLE	99% Confidence Level
El Niño Years	0.83	0.81	0.64	0.52
All Years	0.73	0.70	0.51	0.26

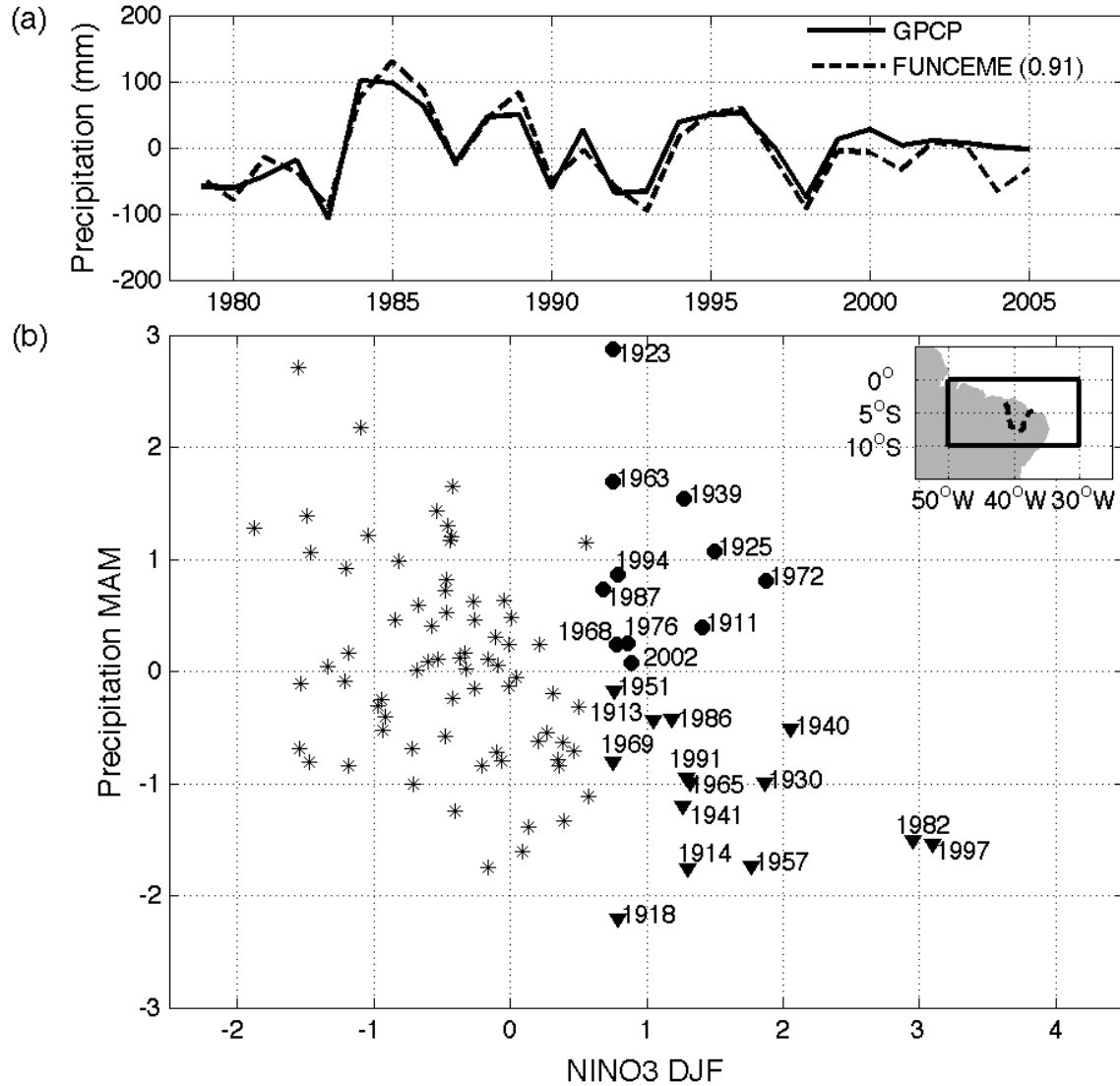


FIG. 1. (a) Precipitation averaged over March-May (MAM) estimated from GPCP dataset (solid line) and FUNCEME dataset (dashed line) for 1979-2005. (b) Scatterplot of NINO3 index (boreal winter, DJF) and NE precipitation from FUNCEME (boreal spring, MAM). Anomalies are normalized by their standard deviations ( $0.93^{\circ}\text{C}$  and  $60\text{ mm}$ , respectively). Asterisks represent non El Niño years. Moderate to extreme El Niño are represented by triangles (circles) when precipitation is below (above) the average. Note that they are labeled by the year corresponding to December of the onset year. Top corner shows area over which

precipitation was estimated: solid box for the GPCP dataset and dashed line for the FUNCEME dataset.

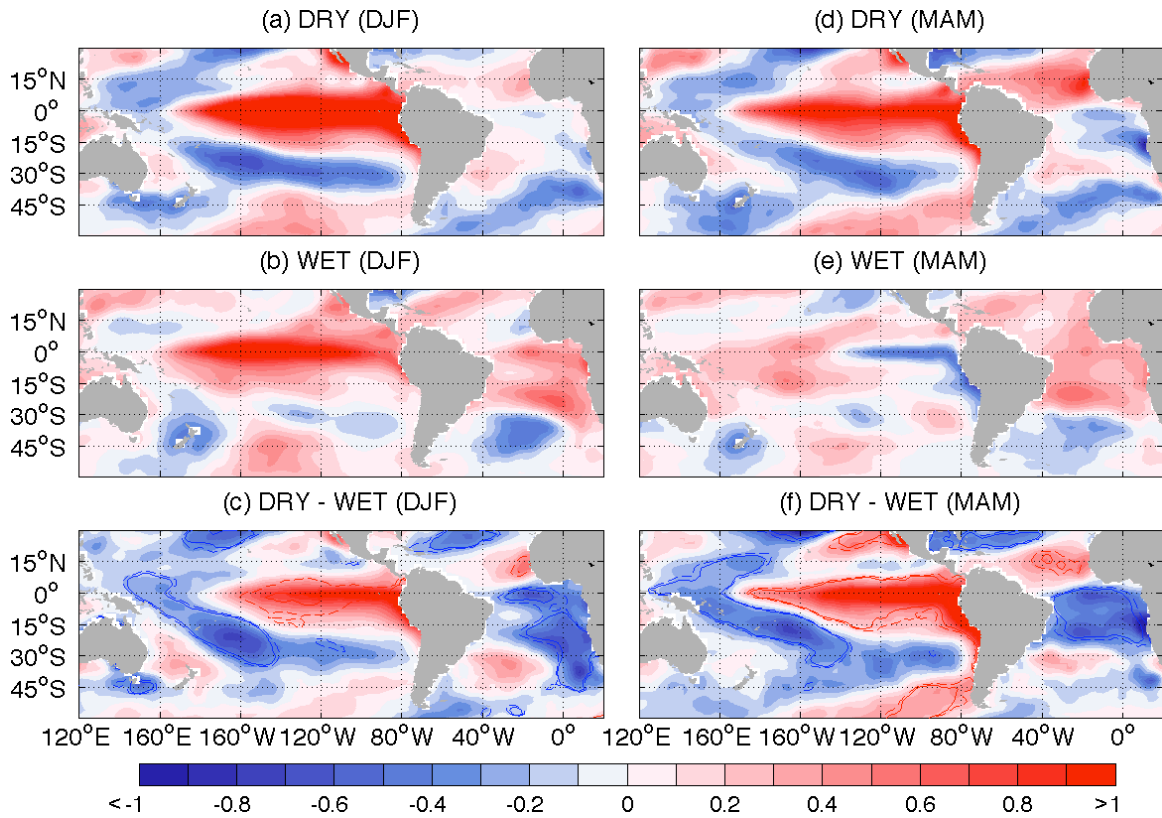


FIG. 2. Composites of SST anomaly ( $^{\circ}\text{C}$ ) in DJF for El Niño years in which the precipitation over the NE is (a) below the average (“DRY”) and (b) above the average (“WET”) for the period of 1957-2002. (c) DRY minus WET composites of SST anomalies in DJF. (d), (e), and (f) same as (a), (b), and (c), except for MAM. Solid and dashed lines in (c) and (f) encompass areas where the difference between the means of the anomalies in DRY and WET El Niño years are statistically significant at 99% and 95% confidence levels, respectively.

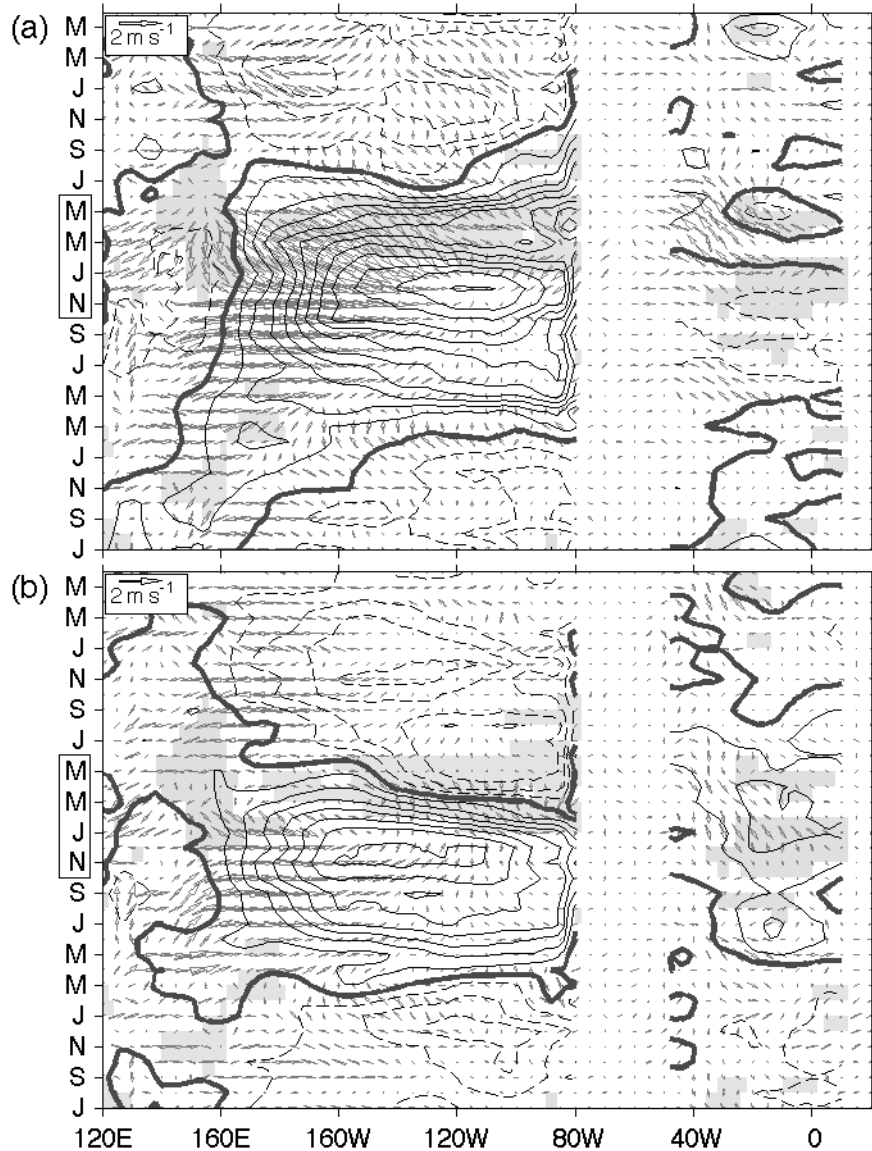


FIG. 3. Hovmuller diagrams of SST anomalies (contours, in  $^{\circ}\text{C}$ ) and near surface wind anomalies (arrows, in  $\text{m s}^{-1}$ ) averaged between  $2.5^{\circ}\text{S}$  and  $2.5^{\circ}\text{N}$  for 1957-2002: (a) composite of DRY El Niño years; (b) composite of WET El Niño years. The contour interval is  $0.2^{\circ}\text{C}$ . Thick solid lines represent zero contours. Shading indicates where the difference between the means of the anomalies in DRY and WET El Niño years are statistically significant at 95% confidence level. Months within the rectangle represent the El Niño mature phase (NDJF) and subsequent rainy season in the NE (MAM).

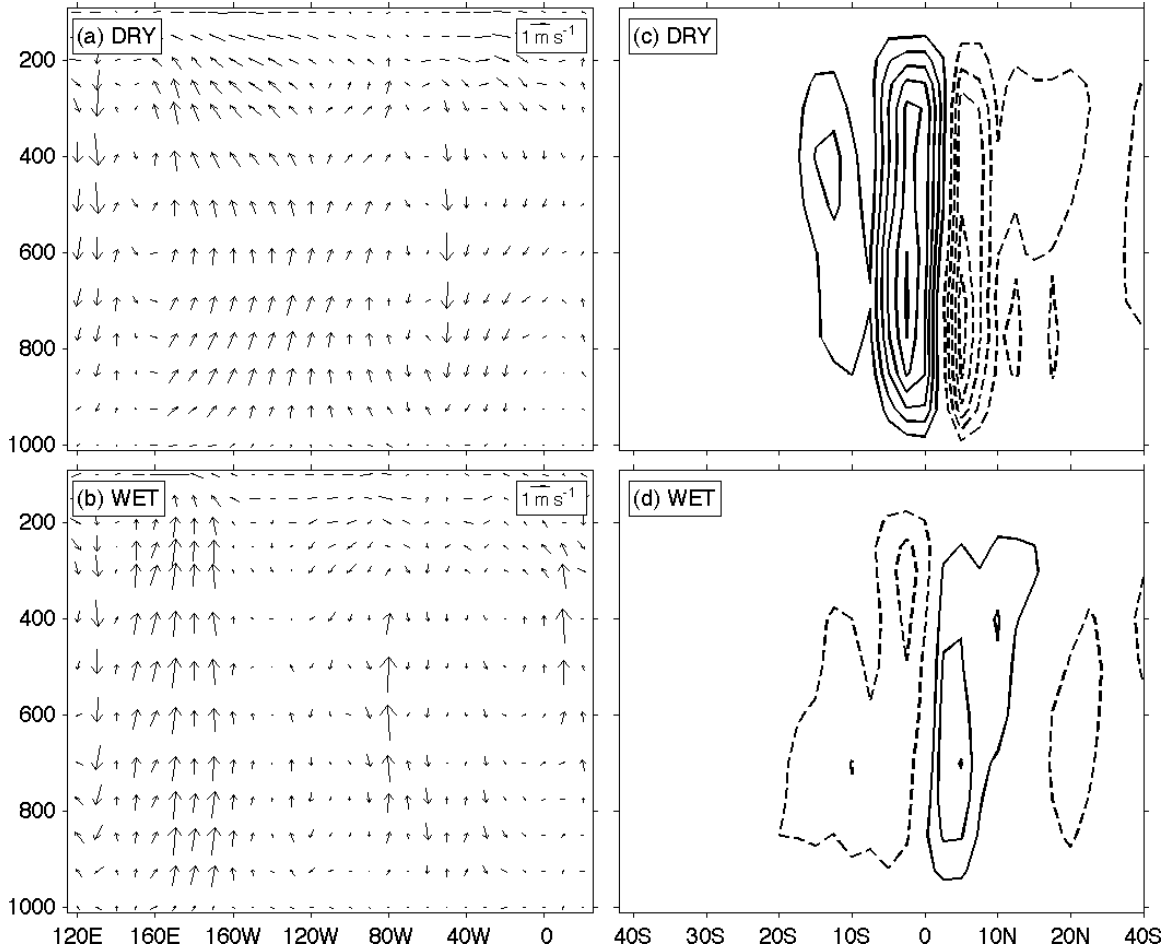


FIG. 4. Walker circulation anomalies by averaging zonal divergent wind and vertical velocity anomalies between  $2^{\circ}\text{S}$  and  $2^{\circ}\text{N}$  for JFMA ( $\text{m s}^{-1}$ ,  $\text{hPa s}^{-1}$ ): (a) composite of DRY El Niño years; (b) composite of WET El Niño years. Hadley circulation anomalies by averaging vertical velocity between  $50^{\circ}\text{W}$  and  $0^{\circ}\text{E}$  for MAM ( $\text{hPa s}^{-1}$ ): (c) composite of DRY El Niño years; (d) composite of WET El Niño years. The contour interval is  $0.5 \text{ hPa s}^{-1}$ . Dashed lines indicate negative values (upward motion). The zero contour is omitted.

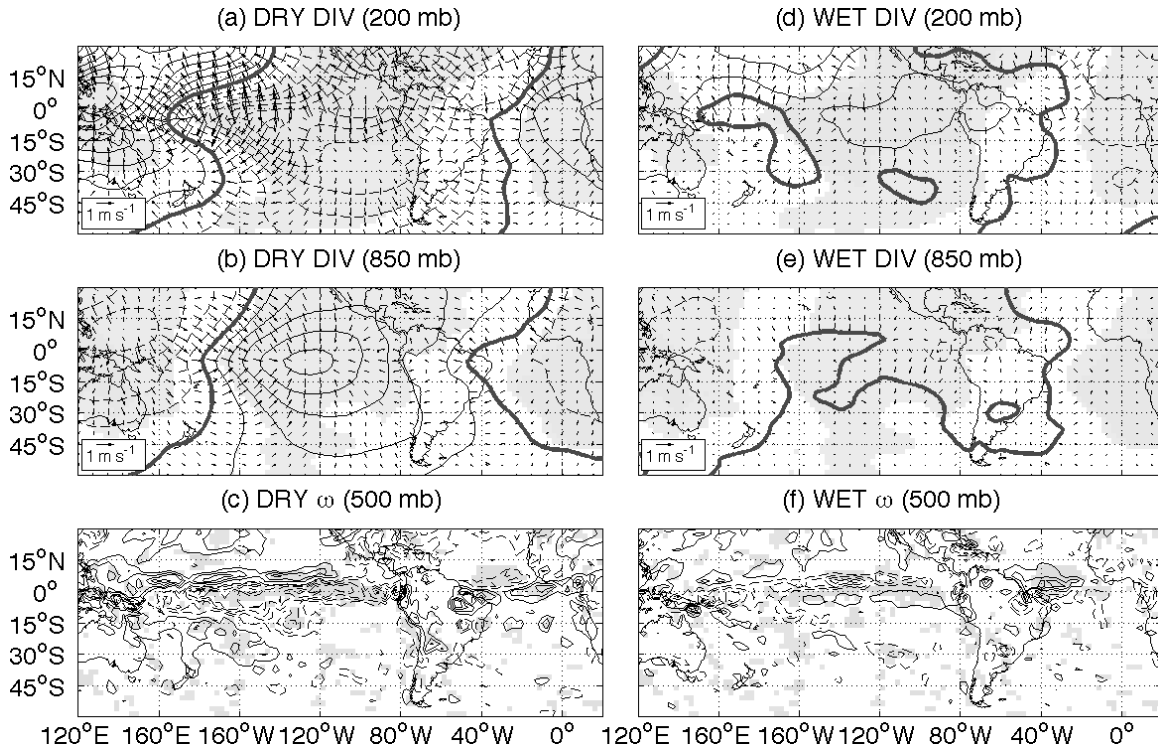


FIG. 5. Composites for DRY El Niño years in JFMA: (a) 200-hPa velocity potential anomalies ( $10^6 \text{ m}^2 \text{ s}^{-1}$ ) and divergent wind anomalies ( $\text{m s}^{-1}$ ); (b) 850 hPa velocity potential anomalies ( $10^6 \text{ m}^2 \text{ s}^{-1}$ ) and divergent wind anomalies ( $\text{m s}^{-1}$ ); (c) 500-hPa vertical velocity anomalies ( $\text{hPa s}^{-1}$ ). (d), (e), and (f) same as (a), (b), and (c) except for WET El Niño years. The contour interval is  $0.5 \times 10^6 \text{ m}^2 \text{ s}^{-1}$  for (a), (b), (d), (e) and  $1 \text{ hPa s}^{-1}$  for (c), (f). Thick solid lines represent zero contours. Shading indicates where the difference between the means of the anomalies in DRY and WET El Niño years are statistically significant at 95% confidence level.

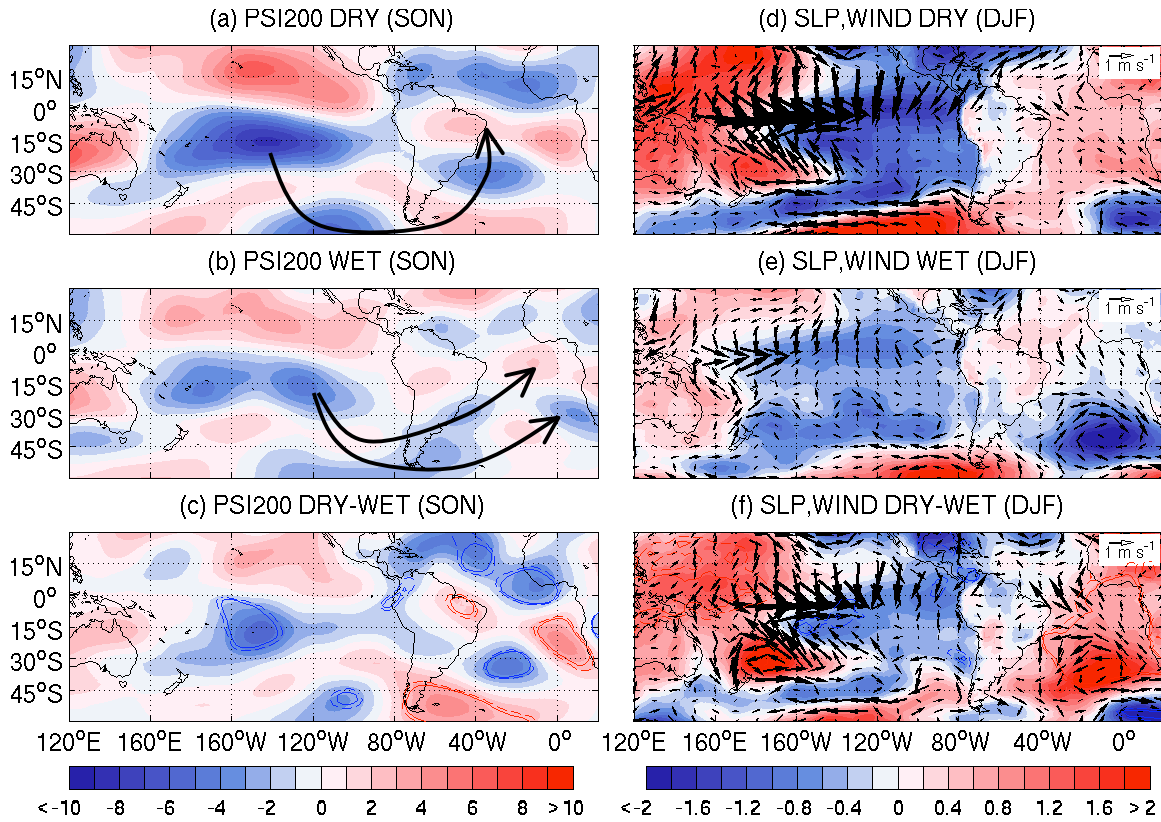


FIG. 6. Composites of eddy streamfunction at 200 hPa ( $10^6 \text{ m}^2 \text{ s}^{-1}$ ) in SON for (a) DRY, (b) WET, and (c) DRY minus WET. (d), (e), and (f) same as (a), (b), and (c), except for sea level pressure (contours, in hPa) and near surface wind (vectors, in  $\text{m s}^{-1}$ ) in DJF. Solid and dashed lines in (c) and (f) encompass areas where the difference between the means of the anomalies in DRY and WET El Niño years are statistically significant at 99% and 95% confidence levels, respectively.

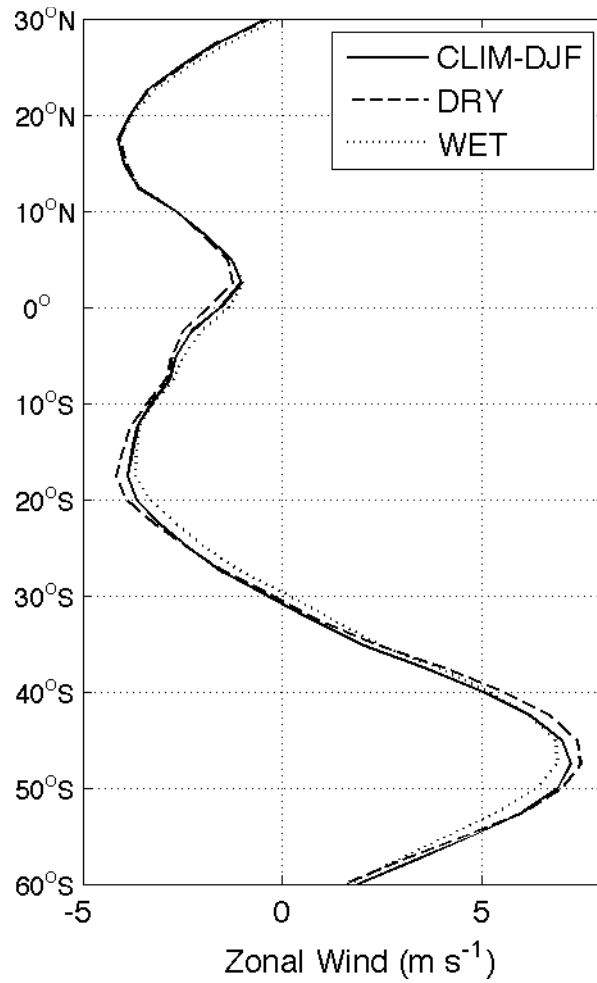


FIG. 7. Zonal wind zonally averaged over the Atlantic between 40°W and 0°E: DJF climatology (solid line), DRY El Niño years (dashed line), and WET El Niño years (dotted line).

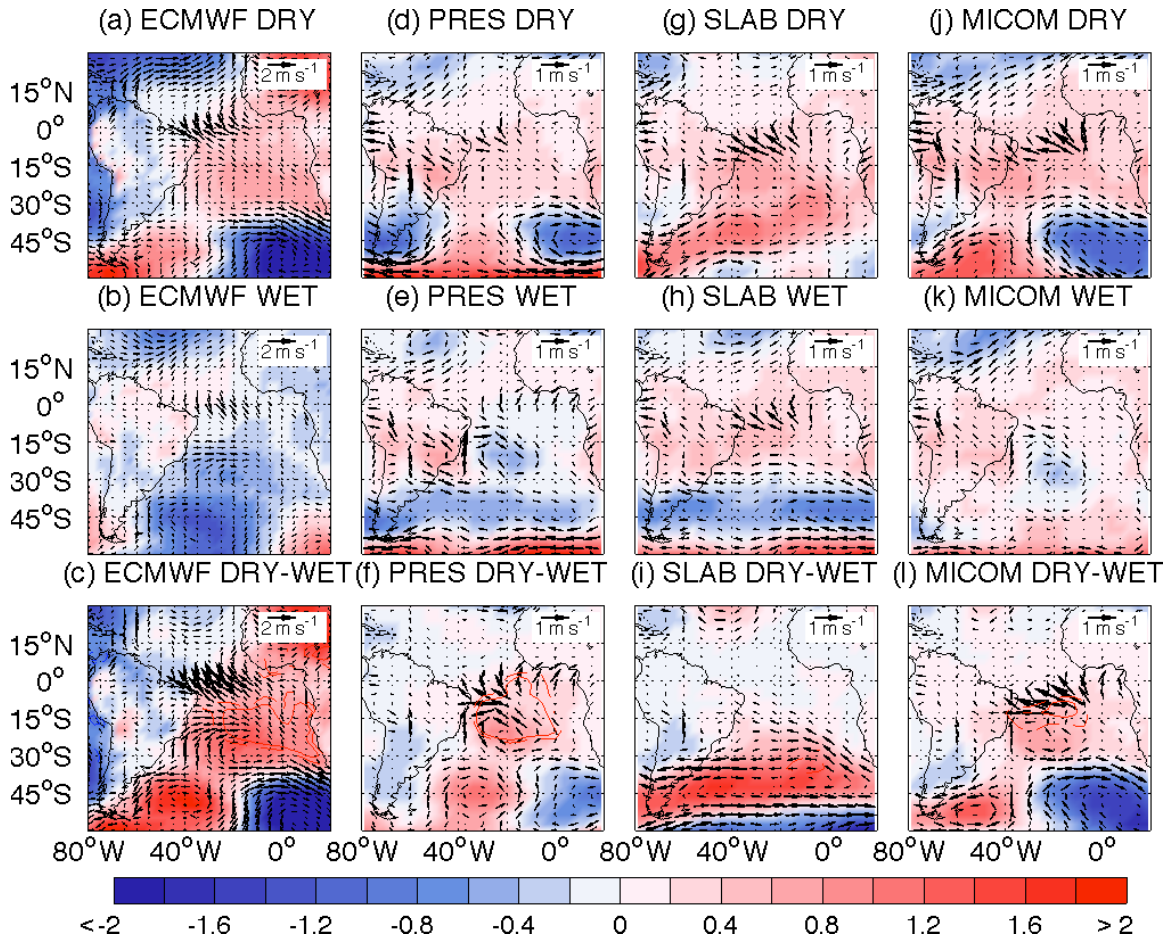


FIG. 8. Sea level pressure (contours, hPa) and near surface wind (vectors,  $\text{m s}^{-1}$ ) in JFMA from observations (a) composites for DRY El Nino years, (b) composites for WET El Nino years, (c) DRY-WET; from the prescribed SST model run (d) DRY run, (e) WET run, (f) DRY-WET runs. (g), (h), (i) and (j), (k), (l) same as (d), (e), (f), except for SLAB and MICOM runs, respectively. Solid and dashed lines encompass the regions where the differences between DRY and WET composites are statistically significant at the 99% and 95% confidence level.

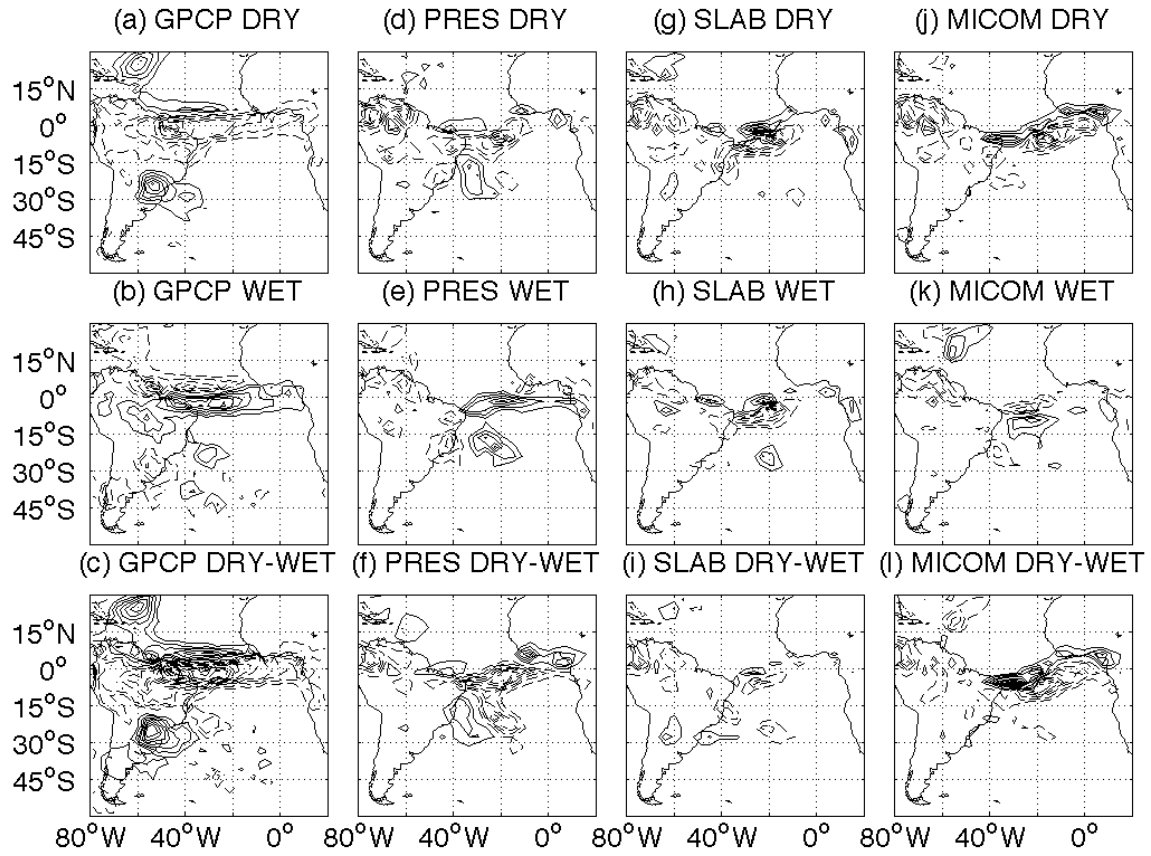


FIG. 9. Same as Fig. 8, except for precipitation ( $\text{mm day}^{-1}$ ) in MAM. The contour interval is  $0.5 \text{ mm day}^{-1}$ . Shown in (c), (f), (i), and (l) contours where the differences are statistically significant at the 95% confidence level.

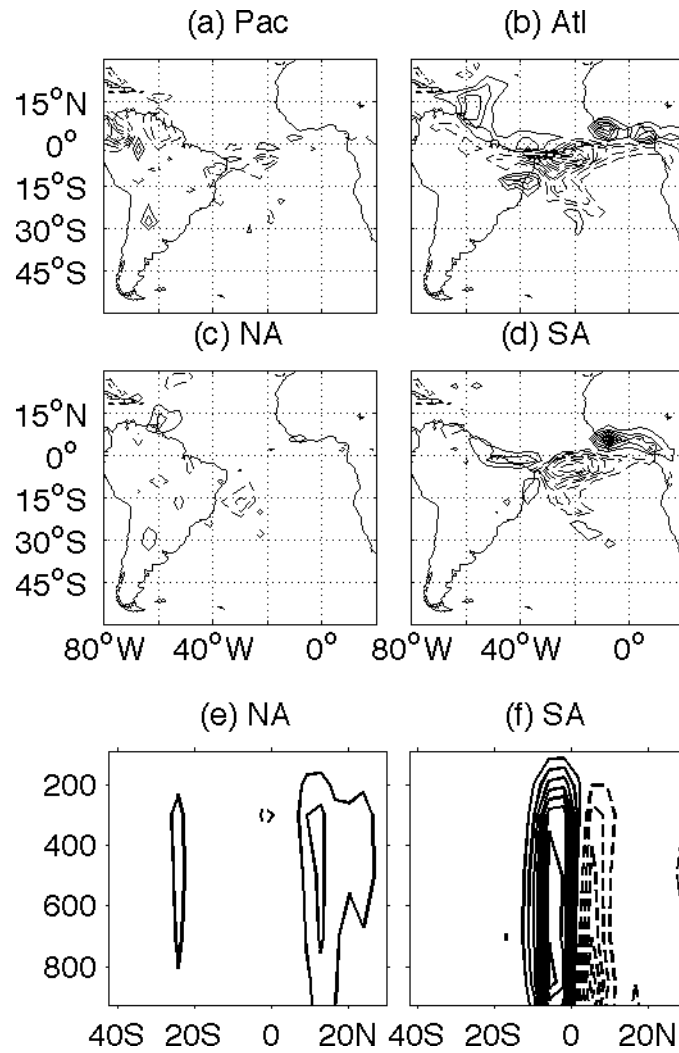


FIG. 10. Precipitation ( $\text{mm day}^{-1}$ ) in MAM from the DRY minus WET runs where the SST anomalies were prescribed only in: (a) Pacific, (b) Atlantic, (c) North Atlantic, and (d) South Atlantic. The contour interval is  $0.5 \text{ mm day}^{-1}$ . (e), (f) same as (c), (d) except for vertical velocity averaged over  $50^{\circ}\text{W}-0^{\circ}\text{E}$  for MAM ( $\text{hPa s}^{-1}$ ). The contour interval is  $0.2 \text{ hPa s}^{-1}$ . Dashed lines indicate negative values (upward motion). The zero contour is omitted.

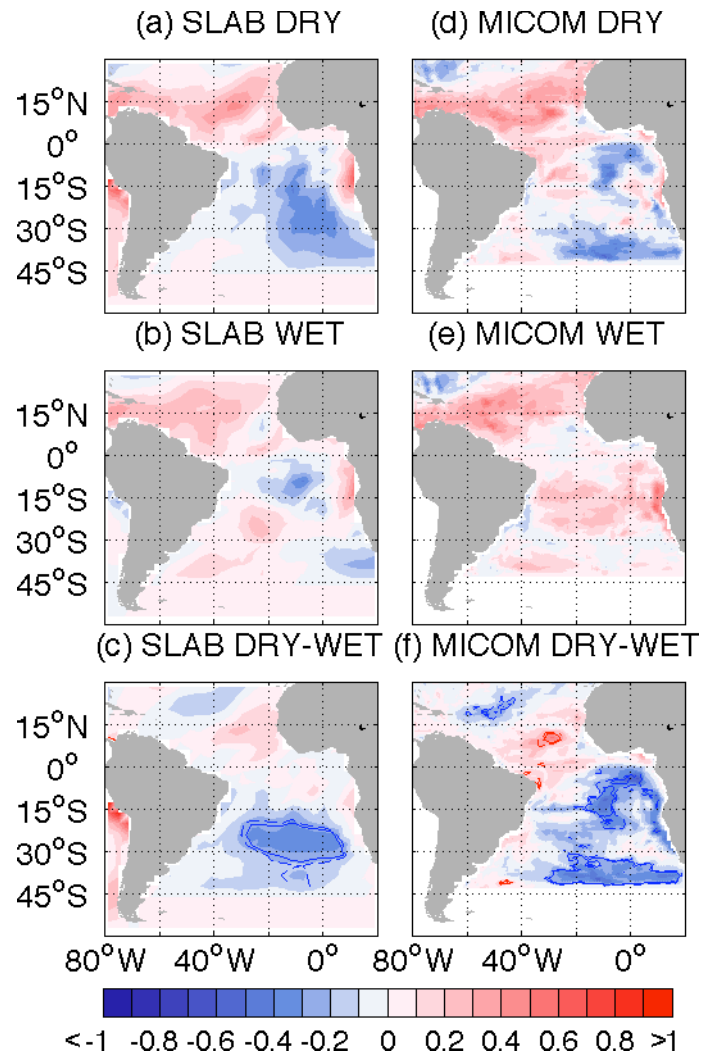


FIG. 11. SST anomalies in MAM from SPEEDY-SLAB: (a) DRY run, (b) WET run, (c) DRY-WET runs; and from SPEEDY-MICOM: (d) DRY run, (e) WET run, (f) DRY-WET runs. Solid and dashed lines encompass the regions where the differences between DRY and WET runs are statistically significant at the 99% and 95% confidence level.

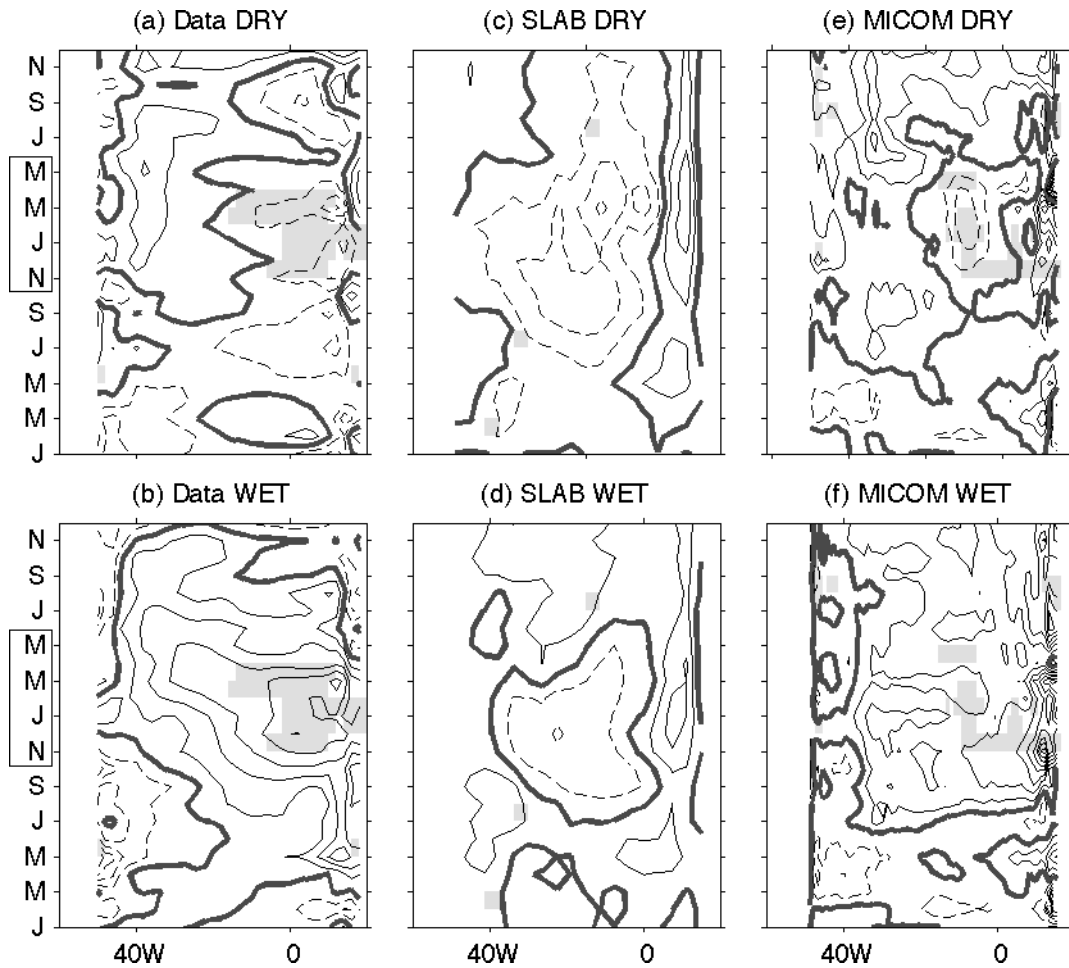


FIG. 12. Hovmuller diagrams of SST anomalies (contours, in  $^{\circ}\text{C}$ ) averaged between  $30^{\circ}\text{S}$  and  $0^{\circ}\text{N}$  from observation: composite of (a) DRY and (b) WET El Niño years; from the SLAB (c) DRY and (d) WET runs; from the MICOM (e) DRY and (f) WET runs. The contour interval is  $0.1^{\circ}\text{C}$ . Thick solid lines represent zero contours. Shading indicates where the difference between the means of the anomalies in DRY and WET El Niño years are statistically significant at 95% confidence level. Months within the rectangle represent the El Niño mature phase (NDJF) and subsequent rainy season in the NE (MAM).

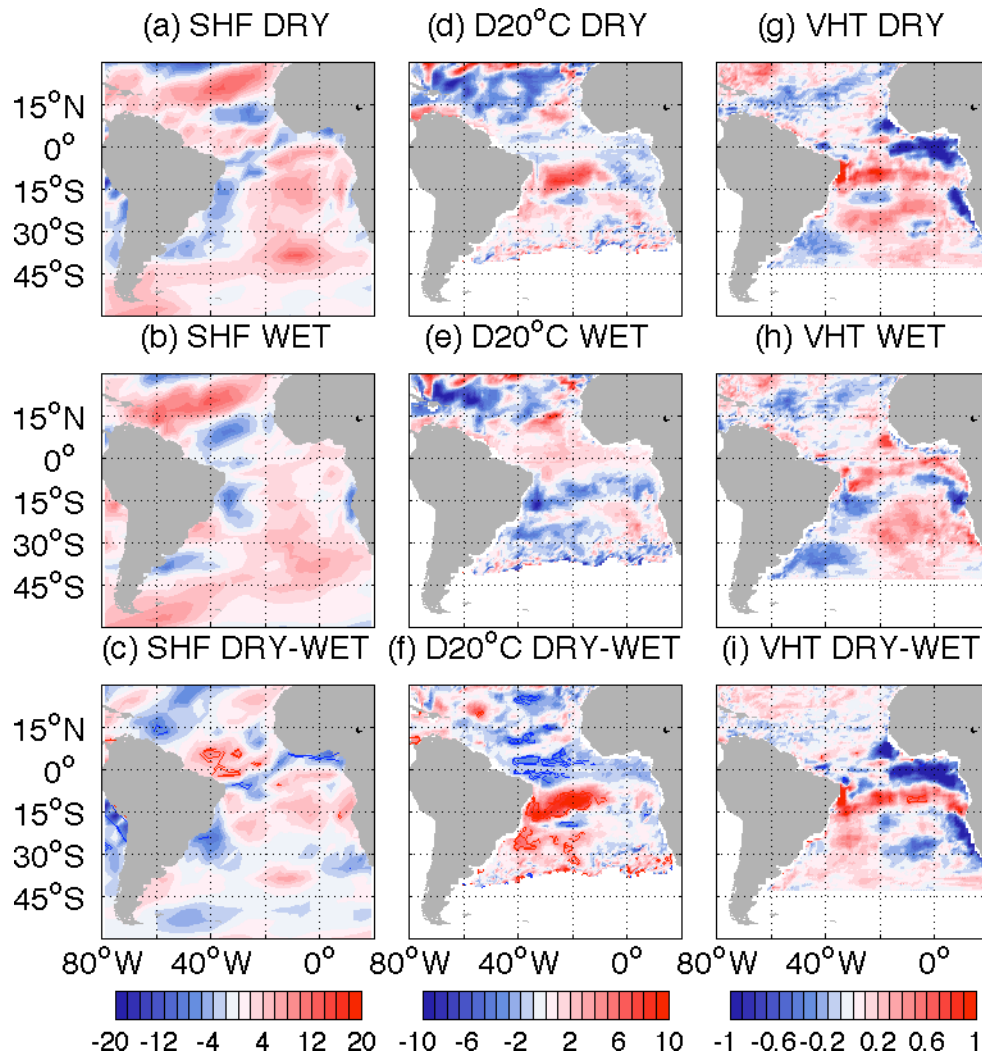


FIG. 13. Net surface heat flux ( $\text{W m}^{-2}$ ) in MAM from the SPEEDY-MICOM: (a) DRY run (b) WET run, and (c) DRY-WET runs. (d), (e), (f) and (g), (h), (i) same as (a), (b), (c), except for depth of the  $20^\circ\text{C}$  isotherm (m) and vertical heat transport ( $\text{K s}^{-1}$ ), respectively. Solid and dashed lines encompass the regions where the differences between DRY and WET runs are statistically significant at the 99% and 95% confidence level.